A Polytopal Element Framework for Improved Solution Accuracy and Robustness

By

Brian Doran Giffin
B.S. (University of California, Davis) 2013
M.S. (University of California, Davis) 2014

Dissertation

Submitted in partial satisfaction of the requirements for the degree of

Doctor of Philosophy

in

Civil and Environmental Engineering

in the

Office of Graduate Studies

of the

University of California

Davis

Approved:

Mark M. Rashid, Chair

N. Sukumar

Boris Jeremić

Committee in Charge

2017

To Lyle . . .

for teaching me how to think deeply, to analyze new information objectively, and to appreciate the complexity and nuanced beauty in all things.

And to Nancy . . .

for inspiring me to explore my creativity, for giving me canvases to paint on, and the confidence to paint, without fear of failure.

Contents

List of Figures

List of Tables

Abstract

A Polytopal Element Framework for
Improved Solution Accuracy and Robustness

A high-level discussion of the fundamental problems accompanying finite element discretizations in the form of locking, addressing the scope of the work under consideration.

Acknowledgments

Many thanks to the following: Professor Amit Kanvinde who inspired much of my initial motivation for applying to graduate school; Professor N. Sukumar for exposing me to the realm of computational solid mechanics; Dr. Joseph Bishop at Sandia for being involved in my early (and continuing) development in the field of solid mechanics; Professor Mark Rashid who turned my spark of interest in the subject into a roaring fire of passion; Dr. Steven Wopschall and Mr. Omar Hafez for being my mentoring older brothers throughout my journey in graduate school; Mr. Subhajit Banerjee and Mr. Eric Chin whose fruitful discussions assisted greatly in developing a personal sense of calm and confidence prior to my qualifying examination; Professor Yannis Dafalias, Professor John Bolander, and Professor Elbridge Puckett, whose enthusiasm as lecturers and courtesy as QE examiners were indespensible; Dr. Joseph Jung, Dr. Kendall Pearson, Dr. Nathan Crane, Mr. Mark Merewether, Dr. Michael Tupek, and the whole of the Sierra Solid Mechanics Team at Sandia who introduced me to the fascinations of code development; Ms. Carly Arthur, Mr. Sam Mish, and Ms. Aimée Sylvia whose conversations as fellow class-mates and advisees were incredibly helpful and insightful; and foremost to Ms. Maha Kenawy, who has served as my primary role-model and source of inspiration for completing this thesis – I love you.

Chapter 1

Introduction

For decades, finite element methods (FEM) have been widely used by engineers and physicists in the modeling of solid continua, and numerous extensions of the method have been developed to model more complex physical processes, including nonlinear kinematic and material behavior. In spite of these advances, traditional finite element methods have been plagued by recurrent issues of numerical accuracy pertaining to locking and poor mesh quality. Various strategies have been proposed to overcome some of these issues, though few have been able to address the underlying problem of element distorsion sensitivity.

This thesis presents a novel polytopal element framework in an effort to address the aforementioned issues as a whole. The use of arbitrary polygonal and polyhedral shapes in place of canonical element shapes seeks to resolve the issue of distorsion sensitivity directly, obviating issues of meshing and mesh quality, while maintaining many of the desirable features of the FEM and its extensions.

1.1 Historical Development

According to [16], finite element methods originated in the 1950s to address engineering challenges in the design of aircraft. The method was subsequently given a more rigorous mathematical treatment by early contributors (Irons, Melosh, Strang), and its usage permeated to other fields of study (namely, structural engineering). Following the advent of the isoparametric element concept, displacement-based finite element formulations gained

widespread popularity, though most early applications considered only linear kinematic and material behavior. Subsequently, advanced solution methodologies were developed to accomodate various sources of nonlinearity, including finite deformations, nonlinear constitutive behavior, and contact.

Over half a century after its initial development, the finite element method is still widely used, and recognized as the industry standard technology for modeling complicated structural and dynamic systems. It's reigning popularity can be attributed to several desirable features of the method:

- The compact support property of the isoparametric basis functions helps to facilitate more efficient solution methodologies.

- The kronecker delta property and precise description of mesh boundaries allow for a relatively straightforward application of boundary conditions and contact constraints.

- Numerical quadrature on element domains derived from product Gauss rules balances accuracy, efficiency, and stability. Domain quadrature rules also naturally accomodate nonlinear kinematic behavior and "black box" constitutive models.

However, despite these advantageous characteristics, finite element methods have suffered from two major (related) issues:

I.) Standard element formulations are prone to the effects of numerical locking phenomena which can significantly degrade the accuracy of the method. These issues are more prevalent for low-order elements, and especially so for linear triangles and tetrahedra. Moreover, very thin or distorted elements tend to exhibit more severe pathologies.

II.) The process of meshing complex geometries is encumbered by the aforementioned concerns over locking, to the extent that it becomes difficult – if not impossible to produce quality discretizations using automated tools which do not require extensive human intervention.

Despite recent efforts to pursue automated quad-dominant [37] and hex-dominant [20] meshing algorithms which seek to optimize certain mesh quality metrics, the inherrent problem of element distorsion sensitivity still remains. Consequently, substantial efforts have been made to address the locking problem through a variety of different approaches. An overview of locking and its remedies are given in the following section.

Locking in Finite Elements

Locking, as a general phenomenon presented in [3], is characterized by a loss of solution accuracy and/or convergence for particular choices of material or discretization parameters. In mathematical terms, an approximation method is deemed *robust* (with respect to a given problem parameter) if its numerical solution converges "uniformly" to the exact solution under mesh refinement, for all values of the indicated problem parameter. Conversely, a method is said to exhibit *locking* if the accuracy of the numerical solution degenerates as the chosen problem parameter approaches some limiting value.

As a specific example, one of the most commonly discussed and addressed forms of locking in computational solid mechanics is the issue of *volumetric locking*, wherein displacement-based element formulations suffer from a marked loss of accuracy when utilized to model the deformation of nearly incompressible materials. For a linear elastic material model, the parameter dependency in question relates to the Poisson's ratio of the material. Other forms of locking may manifest as a sensitivity to geometric/discretization parameters, including: *shear locking*, which is linked to the aspect ratio of continuum elements subjected to bending-dominated deformations; *membrane locking*, which occurs in curved shell elements (see [51]); and *trapezoidal locking*, which affects the bending response of distorted four-node quadrilateral elements (see [27]).

Early efforts to address concerns over locking sought to develop more robust discretizations through the use of higher-order elements. In [2] and [44], Babuška and Suri justified the ability of high-order elements to overcome the effects of volumetric locking (for triangular discretizations). The improved convergence behavior of these elements made them an attractive option for seeking efficiency gains, as well. Nonetheless, higher-order elements were generally seen as too complex in comparison with the standard low-order

elements commonly used for commercial applications; many cite the relative difficulty of obtaining lumped mass matricies for high-order elements (for explicit dynamics applications). Moreover, the accuracy of high-order isoparametric elements can be severely degraded if the elements posess curved edges, as demonstrated in [24].

As an alternative to the standard displacement-based FEM, some have argued for the use of *mixed finite element methods* (MFEM), which provide a separate interpolation of the displacement, strain, and stress fields, utilizing a 3-field Hu-Washizu variational principle in the construction of the weak form. While these methods are generally seen as robust in the face of locking (as noted in [2] and [3]), they are nonetheless subject to potential issues of stability, i.e. the Babuška-Brezzi – or inf-sup conditions (refer to [1], [5].) Additionally, mixed methods tend to be less efficient in comparison with displacement-based FEM, and are not as flexible in their ability to handle arbitrary constitutive relationships.

In an effort to retain some of the beneficial characteristics of mixed finite element methods, *mixed assumed strain methods* (alternately the *method of incompatible modes*) were formalized for geometrically linear problems in [41], and extended to nonlinear problems in [39] and [40]. Such methods are derived from a 3-field variational principle, and rely upon energy orthogonality between the enhanced strain field and the resulting stress field to eliminate the need for an independent stress interpolation space, thereby yielding a 2-field formulation. Though the method is effective in treating a variety of geometric locking phenomena, it nonetheless leads to spurious instabilities in both linear and nonlinear problems (see [45] and [32], respectively), even for element formulations satisfying the inf-sup conditions.

Other attempts to adapt mixed formulations for more general use with arbitrary material models without relying upon an explicit interpolation of the stress or strain fields have resulted in *selective reduced integration* (SRI) and equivalent *strain projection* techniques. These methods were fairly successful in overcoming the issues of volumetric locking via the B-bar projection approach for linear problems discussed in [22], and via the F-bar approach for nonlinear problems discussed in [13]. Though these methods can be both effective and efficient, their success has been limited to the problem of volumetric locking;

they are less successful with regard to treating other forms of locking, and can lead to stability problems if the strain projection spaces are not selected carefully.

At the opposite end of the spectrum – in recognition of the inherrent issues of stability plauging mixed methods and reduced integration techniques, methodologies employing *orthogonal hourglass control* were suggested, as in [17]. These approaches consider the use of low-order quadrature rules to avoid common locking phenomena, supplemented by artificial stiffness terms to maintain stability while preserving essential convergence characteristics. While these formulations tend to be highly efficient computationally (particularly for explicit dynamic analyses), the obvious disadvantage of these approaches relates to their reliance upon user-specified artificial stiffness and viscosity parameters. Appropriate selection of these parameters is not always a trivial matter, and often warrants problem-specific investigations via sensitivity analyses.

Ultimately, the foregoing methodologies have had only limited success in resolving the full spectrum of locking problems, particularly with regard to geometric locking phenomena. Moreover, many of the proposed enhancements are limited to specific element types (typically low-order quadrilaterals or hexahedra), and are not readily generalizable to other discretizations. To a large extent, the propensity for locking in FEM is controlled by the standard isoparametric elements' sensitivity to geometric distorsion. In other words, model accuracy is too often the product of the chosen discretization. For this reason, considerable efforts have been invested in recent years towards the development of alternative discretizations and numerical methods, a few of which are discussed in the following section.

Alternative Numerical Methods and Discretizations

Driven by concerns over meshing and element quality, a wide variety of alternative approximation methods have been explored in recent decades. The general consensus is that the construction of an approximation space should be disconnected (to a variable extent) from the particular choice of discretization. In particular, isoparametric finite element basis functions are conveniently defined in terms of the discretization, but may not necessarily result in a suitable approximation space for the given problem at hand.

In direct response to these considerations, so-called *meshfree* methods were developed in an effort to construct approximation spaces that are defined independently of a chosen spatial discretization. Meshfree methods encompass a broad class of approximation schemes, including smoothed particle hydrodynamics (SPH), the element-free Galerkin (EFG) method, and the reproducing kernel particle method (RKPM), among others. A majority of these methods rely upon an a priori specification of weighting functions used to construct an associated set of polynomially reproducing basis functions. The resulting meshfree basis yields relatively smooth solutions which are less sensitive to the specific choice and distribution of weighting functions.

The departure from defining an approximation space on a structured partition of the domain presents a number of challenges, however. Specifically, meshfree methods still require the definition of a background mesh to effect numerical integration of the weak form, partially invalidating the namesake of the method. Moreover, because the meshfree basis functions tend to be non-polynomial in form (and because they are not compactly supported/overlapping on element domains), they are more challenging to accurately integrate. Chen et. al. have proposed a means of overcoming these issues in [6] through a *variationally consistent integration* scheme, though this approach is succeptible to numerical instabilities. Additionally, because the basis functions do not in general exhibit the kronecker delta property, the application of boundary conditions and contact constraints becomes less straightforward; several techniques have been proposed to address this issue, including Lagrange multiplier methods, Nitsche's method, and mesh blending at domain boundaries.

As another alternative, *discontinuous Galerkin* (DG) methods have gained recent attention due to their more flexible represention of solution fields as piece-wise polynomials over individual elements, resulting in solution discontinuities at element boundaries. To stabilize the resulting approximation space, DG methods supplement the weak form with interior penalty terms which seek to minimize these discontinuities. DG methods are advantageous in that they may accomodate arbitrary element shapes, and exhibit desireable distorsion robustness characteristics.

DG approaches are not without their own problems, however. One commonly cited issue relates to the fact that DG methods can become sensitive to the choice of penalty parameters used to weakly enforce inter-element continuity and boundary conditions; the selection of these parameters is problem dependent. Additionally, DG methods tend to suffer from poor numerical conditioning problems if the discretization does not conform with relatively stringent regularity requirements, thereby limiting the types of discretizations used with the method.

The more recent *weak Galerkin* (WG) finite element method first introduced by Wang and Ye for elliptic problems in [49], and for parabolic equations by Li and Wang in [25], considers an approximation space consisting of functions defined on polygonal element domains which are consistent with the weak gradient of functions independently defined on shared element edges. The discrete approximation spaces under consideration are typically low-order polynomials (commonly just constants) defined on elements and their edges. However, there are some non-trivial choices that must be made regarding an optimal selection of these polynomial spaces for the sake of computational efficiency (discussed in greater detail in reference [31]). The method has so-far only been applied to the solution of linear problems.

The computational accuracy of the weak Galerkin approach has been explored by Mu et. al. in [29], showing that for certain problems, the weak Galerkin method converges at rates comparable to those of the standard FEM. Lin et. al. performed a comparative study between the weak Galerkin, discontinuous Galerkin, and mixed finite element methods in [26], demonstrating some of the competitive and desirable characteristics of WG in contrast to DG or MFEMs (i.e. no need for penalty parameters, and definiteness of the resulting linear system of equations).

Mu et. al. adapted the method for use on arbitrary polytopal meshes in [30] and [31], albeit with a number of shape regularity restrictions placed on the elements. In general, the implementation of WG considers the mesh degrees of freedom as belonging to both the elements and their edges, however in [31] it is noted that the local element degrees of freedom can be expressed in terms of the bounding edge degrees of freedom alone to

improve computational efficiency. A modified approach by Wang et. al. in [50] instead chooses to express functions on edges only implicitly. Although this approach successfully eliminates the computational expense associated with edge-based degrees of freedom, it requires the inclusion of an additional interior penalty term in the weak form, similiar to a discontinuous Galerkin method.

In the wake of these investigations, it became clear that many of the desirable properties of the FEM (compact support, kronecker delta, quadrature efficiency, DoF efficiency, stability, and inter-element compatibility) were qualities worth preserving. To this end, efforts were made toward improving and generalizing existing element formulations for arbitrary element shapes – polygons and polyhedra. Rather than relying upon shape functions defined through an isoparametric transformation from a parent element domain, recent polytopal element methodologies have explored various techniques for constructing approximants directly on physical element domains. In doing so, issues regarding distorsion sensitivity of the elements are largely obviated, and new opportunities for discretizing the domain with irregular shapes are made possible. In like fashion, recent advances in meshing technologies have made polyhedral element methods a readily feasible option. Very recently, Ebeida et. al. have released VoroCrust ([15]): a robust voronoi discretization tool based on constrained Poisson disk sampling. Concurrent technologies have also advanced polyhedral mesh generation via boolean intersection of a background hexahedral mesh with a piece-wise linear boundary representation (or B-rep).

For these reasons, efficient and robust polyhedral element formulations are in high demand, leading to a proliferation of new approaches. A number of these are discussed in the following section.

1.2 Recent Developments in Polytopal Discretizations

Polytopal element methods combine many of the attractive features of FEM with the geometric flexibility afforded by arbitrary element shapes, the primary motivation for which arises from the aforementioned concerns over discretization sensitivity. Most of these methods share a few distinguishing features in common with one another: mesh

degrees of freedom are borne by nodes – the geometric verticies of (low-order) elements; nodal basis functions are compactly supported over adjoining element domains, and satisfy the kronecker delta property; basis functions are defined directly on the element's physical domain, rather than on a parent domain.

Where these methods differ is in the way that they choose to define an element's shape functions (if at all). These approaches may be loosely organized into three distinct categories: methods which explicitly define the element's basis functions via a continuous interpolation scheme; methods which define the element's shape functions only implicitly – i.e. "virtual" element methods; and methods which form a discrete representation of the element's shape functions via an approximation scheme. These three methodologies are elaborated upon in the following sections.

Continuous Interpolation on Arbitrary Polytopes

In an effort to generalize the core idea behind isoparametric element coordinates which yield a point-wise definition of the element's shape functions and their gradients within a given element domain, various efforts to explicitly define shape functions directly on arbitrary polytopal domains has led to the creation of a broad family of interpolation schemes, collectively referred to as *generalized barycentric coordinates*.

At a minimum, shape functions which fall into this category must: form a partition of unity, satisfy linear completeness, and interpolate the nodal data (i.e. satisfy the kronecker delta property). These coordinates are uniquely defined according to the standard barycentric coordinate system for simplicial domains. For arbitrary polytopal domains, numerous such coordinate systems exist, including Wachspress' coordinates [48], mean values coordinates [18], harmonic coordinates [23], and maximum entropy coordinates [43], among others.

Though generalized barycentric coordinates have been applied in the context of finite elements, their development has largely been propelled by the graphics community on account of their relatively smooth interpolatory properties. However, thier smooth (non-polynomial) character presents a challenge with regard to accurate numerical integration. Consequently, relatively high-order quadrature schemes are required to achieve reason-

able accuracy and satisfaction of patch tests. More recently, a polynomial projection scheme has been suggested in [46] to remedy these integration errors for linear problems; for general nonlinear problems, a gradient correction scheme has been proposed in [47] and [8]. These developments have illuminated new possibilities for defining more efficient quadrature rules on polytopes while still satisfying the essential requirements for convergence.

Yet in spite of these developments, many existing coordinate schemes are sill limited by moderate to severe restrictions on element shape/convexity, and produce sharp gradients in the presence of degenerate geometric features. These concerns, and a recognition of the fact that the shape functions need not be defined point-wise for finite element applications, have motivated research efforts toward discrete representations of element interpolants.

Virtual Element Methods

The *virtual element method* (VEM) summarized in [11] is a relatively new approach, and based in part upon the older concept of mimetic finite differences (MFD). Although the method supposes that continuous basis functions *exist* within arbitrary polytopal elements, the VEM never explicitly *defines* how these shape functions vary on element interiors. Instead, the VEM supposes that these "virtual" functions may be separated (via projection operators) into polynomial and non-polynomial parts, which are handled in different ways. The cornerstone of the method is the idea that the bilinear form for a given element may be decomposed into two distinct parts: a term which guarantees variational consistency (Galerkin exactness) involving the low-order polynomial part of the shape functions, and a term which provides stability involving the non-polynomial part. The consistency term must be integrated exactly, but the stability term can be evaluated approximately. Because this decomposition relies upon the linearity of the bilinear form, direct generalizations of the method to nonlinear problems are not immediately available.

VEM has been applied to three-dimensional linear elasticity problems in [19]. In [12], a VEM formulation for low-order elements which accomodates nonlinear "black-box" constitutive algorithms is presented, and in [7] an extension to finite deformations (with appropriate stabilization terms) is introduced. Given the means by which these

approaches exploit the use of a projected uniform gradient to integrate the weak form, however, it is unclear how they could be extended to accomodate higher-order elements.

Nonetheless, VEM formulations are able to tolerate geometric degeneracies and element non-convexity without encountering serious numerical difficulties, though their good behavior in the presence of these features is often governed by an ad hoc approximation of the stabilization terms. A more rigorous development of the corresponding stability terms for more complicated element domains remains to be explored.

Approximate Interpolation on Arbitrary Polytopes

In contrast with the previously described approaches, yet another strategy considers the representation of the element's shape functions in an approximate way, while enforcing a few essential requirements, namely: polynomial reproducibility, inter-element compatibility, and weak form consistency.

In [34] and [36], Rashid and co-workers explored the *variable element topology finite element method* (VETFEM), characterized by an approximate representation of the element's shape functions as low-order polynomials satisfying weak continuity requirements at element boundaries. Within this framework, the element shape functions are determined by a local minimization problem, resulting in polynomial shape functions which optimize specified continuity and smoothness objectives. This minimization procedure is constrained by the requirements of consistency and reproducibility to guarantee satisfaction of linear patch tests. Dohrmann and Rashid later extended this approach to higher-order elements in [14], instead focusing on a direct construction of shape function derivatives, rather than of the shape functions themselves.

The VETFEM may be viewed as a non-conforming finite element method, as the minimization process altogether allows for residual discontinuities at inter-element boundaries. Nonetheless, because the elements satisfy weak contunity requirements, the method exhibits proper convergence characteristics. Additionally, because the VETFEM yields a point-wise representation of the shape functions as low-order polynomials, direct integration of the weak form can be carried out using relatively efficient domain quadrature rules.

Although the VETFEM was developed to handle arbitrary polygonal elements, it was observed to suffer from sensitivity to geometric degeneracies and element non-convexity. In response to these issues, a *discrete data polyhedral finite element method* (DDPFEM) proposed in [38] was suggested to exploit the fact that for typical solid mechanics applications, it is generally only necessary to evaluate the element's shape functions (and their derivatives) at a discrete number of quadrature points. The proposed method shares several characteristics in common with the VETFEM, utilizing a similarly posed constrained minimization procedure to obtain the precise values and gradients of the shape functions at discrete points on the element's interior. One of the cited challenges with this approach pertains to the appropriate selection of an efficient quadrature rule for the elements.

Nonetheless, the initial thoughts put forward by the DDPFEM ultimately led to the development of the *partitioned element method* (PEM) presented in [35]. The PEM proceeds by partitioning an element into polygonal quadrature cells, and allowing the element's shape functions to vary according to a local polynomial defined within each of these cells, resulting in piece-wise polynomial shape functions which are discontinuous at quadrature cell boundaries. The polynomial coefficients defined in each cell are obtained by minimizing the discontinuities in the shape functions across all cell interfaces, subject to the necessary consistency and reproducibility constraints. The original presentation in [35] considers the shape functions to be approximate solutions of Laplace's equation on the partitioned element. Later developments have dispensed with this supposition, instead only penalizing discontinuities in the shape functions (and their gradients) at cell boundaries.

Subsequently, Bishop has proposed a very similar partitioned element scheme in [4], wherein the elements and their faces are subdivided into simplicies, resembling a local FE discretization of the element domain. The shape functions are obtained as the solution to Laplace's equation on this subdivision. Because this approach utilizes an FE-like discretization, the resulting shape functions are piece-wise linear and C^0 continuous, thereby avoiding the need for a penalty term to enforce continuity. However, the method still requires the use of a gradient correction scheme to account for quadrature error and recover

consistency with the weak form.

In light of these developments, we choose to recognize a new class of methods, herein collectively referred to as *partitioned element methods*. These may be viewed as a generalization of the original PEM presented in [35]. It is the subject of this thesis to further explore these methods, and to expose their particular merits and potential shortcomings.

1.3 Scope of the Present Work

In this work, we put forth a general framework for partitioned element methods – a collection of different approaches for constructing approximate representations of element shape functions on arbitrary polytopes. These methods are characterized by several distinguishing features:

(1) Elements are discretized (partitioned) into non-overlapping polygonal cells. These cells are used to inform the quadrature rule of the element.

(2) A local approximation space is defined on the partitioned element geometry.

(3) A set of BVPs and appropriate constraints are posed, whose solutions yield the shape functions of the element.

(4) A stable numerical scheme is developed to obtain approximate solutions to these BVPs using the approximation space defined in (2).

Numerous formulations are possible within this framework; a few of these are explored within the scope of this thesis.

The proposed application area of interest for these methods is in nonlinear solid mechanics. The efficacy of the methods explored will be assessed within this context, particularly with regard to their ability to naturally accomodate nonlinear kinematic and material behavior. The robustness of the resulting elements, and their performance in the face of locking phenomena will be evaluated. Additionally, several methodologies which leverage the partitioned element framework to combat certain forms of locking will be discussed.

The remainder of this dissertation is organized as follows: chapter 2 establishes the context of nonlinear computational solid mechanics, chapter 3 presents the overarching framework for partitioned element methods, chapter 4 details a particular implementational framework for the PEM, chapter 5 provides a number of numerical investigations of the PEM, and chapter 6 concludes with a discussion of opportunities for further research and development.

Chapter 2

An Overview of Computational Solid Mechanics

This chapter addresess some of the essential aspects of numerical approximation methods for modeling solid continua. The discussion herein will focus on the mathematical foundations of solid mechanics, beginning with the kinematics of motion and some common forms of constitutive relationships, followed by the expressions for conservation of momentum in both strong and weak form, and concluding with an analysis of the standard numerical methods utilized to solve these equations in an approximate sense. In the course of our discussion, we will make explicit the ensuing requirements placed upon any prospective approximation scheme. This will aid our analysis in subsequent chapters, and hopefully justify particular choices made in the construction of partitioned element methods.

2.1 The Lagrangian Description of Motion

Consider a body $\mathcal{B}_0 \subset \mathbb{R}^d$ consisting of a set of material points whose positions in some reference configuration at time $t = 0$ are denoted $\mathbf{X}$. At a later time $t > 0$, the body occupies a new configuration $\chi(\mathcal{B}_0, t) = \mathcal{B}_t \subset \mathbb{R}^d$, such that the motion of individual material points yield new spatial positions $\mathbf{x}$ according to the bijection $\chi_t : \mathbf{X} \leftrightarrow \mathbf{x}$, i.e.

$$\mathbf{x} = \chi(\mathbf{X}, t), \quad \mathbf{X} = \chi^{-1}(\mathbf{x}, t). \tag{2.1}$$

The displacement $\mathbf{u}$ of a given material point may be expressed as $\mathbf{u} = \mathbf{x} - \mathbf{X}$, and it's corresponding velocity is denoted $\mathbf{v} = \dot{\mathbf{x}} = \partial\mathbf{x}/\partial t$. Figure 2.1 provides a visual interpretation of the situation described.

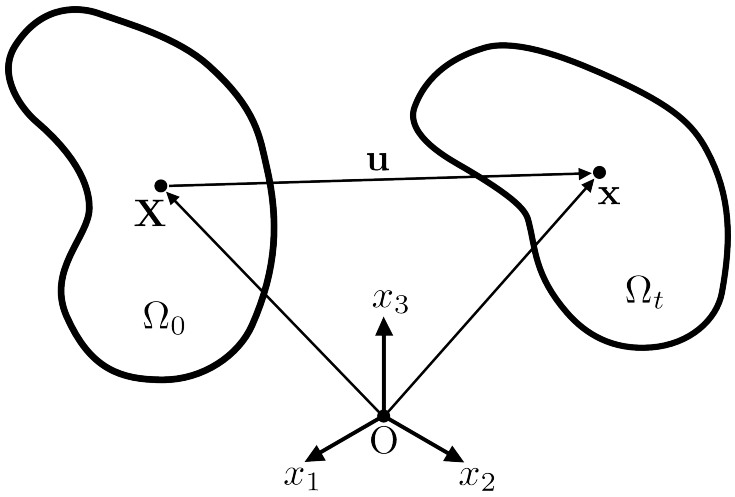

Figure 2.1. A depiction of the motion of material points in a body Ω.

At a given time t, the Jacobian of the deformation mapping χ_t yields the deformation gradient $\mathbf{F} = \nabla_X \mathbf{x}$ (a rank-2 tensor), defined as

$$\mathbf{F} = \frac{\partial \mathbf{x}}{\partial \mathbf{X}} = \mathbf{1} + \nabla_X \mathbf{u}, \tag{2.2}$$

where ∇_X denotes the gradient with respect to $\mathbf{X}$. The deformation gradient may be used to map differential line segments $d\mathbf{X}$, surface areas $d\mathbf{A}$, and volumes dV defined in the reference configuration into their corresponding transformed quantities ($d\mathbf{x}$, $d\mathbf{a}$, dv) at time t:

$$d\mathbf{x} = \mathbf{F} d\mathbf{X}, \quad d\mathbf{a} = J\mathbf{F}^{-T} d\mathbf{A}, \quad dv = J dV, \tag{2.3}$$

where $J \equiv \det \mathbf{F}$.

In like fashion, the spatial velocity gradient $\mathbf{L} = \nabla_x \mathbf{v}$ (where ∇_x denotes the gradient with respect to $\mathbf{x}$) may be expressed as

$$\mathbf{L} = \frac{\partial \mathbf{v}}{\partial \mathbf{x}} = \frac{\partial \dot{\mathbf{x}}}{\partial \mathbf{X}} \frac{\partial \mathbf{X}}{\partial \mathbf{x}} = \dot{\mathbf{F}} \mathbf{F}^{-1}, \tag{2.4}$$

which may be further decomposed into a symmetric part $\mathbf{D}$ (the rate of deformation tensor) and an anti-symmetric part $\mathbf{W}$ (the spin tensor):

$$\mathbf{D} = \frac{1}{2}(\mathbf{L} + \mathbf{L}^T), \quad \mathbf{W} = \frac{1}{2}(\mathbf{L} - \mathbf{L}^T). \tag{2.5}$$

Compatibility

Compatibility refers to the idea that a given body remains a contiguous medium following some deformation described by χ_t. In other words, χ_t must characterize a continuous mapping of material points between different configurations in time, such that the topology of body remains unchanged. Compatibilitiy is characterized by the following necessary and sufficient conditions:

$$\nabla_X \times \mathbf{F} = \mathbf{0} \quad \forall \mathbf{X} \in \mathcal{B}_0. \tag{2.6}$$

Satisfaction of the above compatibility condition implies that there exists a continuous, single-valued displacement field which gives rise to the deformation characterized by $\mathbf{F}$.

Finite Strain Measures

Consider the set of all material line segments $d\mathbf{X}$ which lie in a small neighborhood around a given material point $\mathbf{X}$. Also, consider these same material line segments $d\mathbf{x}$ in the current configuration of the body after some deformation corresponding to $\mathbf{F}(\mathbf{X}, t)$ has taken place, such that $d\mathbf{x} = \mathbf{F} d\mathbf{X}$.

At a given material point $\mathbf{X}$, the deformation gradient $\mathbf{F}(\mathbf{X}, t)$ is a linear operator, which may be decomposed into two step-wise operations: a stretching operation $\mathbf{U}$ (or $\mathbf{V}$), and a rotation $\mathbf{R}$, yielding the polar decomposition of $\mathbf{F}$:

$$\mathbf{F} = \mathbf{R}\mathbf{U} = \mathbf{V}\mathbf{R}, \tag{2.7}$$

where $\mathbf{U}$ is termed the right stretch tensor, and $\mathbf{V}$ is the left stretch tensor. There arise from $\mathbf{U}$ and $\mathbf{V}$ two primary deformation measures: the right Cauchy-Green deformation

tensor $\mathbf{C} = \mathbf{U}^2$, and the left Cauchy-Green deformation tensor $\mathbf{B} = \mathbf{V}^2$. Each of these, in turn, yield the two most commonly utilized finite strain measures: the Green-Lagrangian strain tensor $\mathbf{E} = \frac{1}{2}(\mathbf{C} - \mathbf{I})$, and the Eulerian-Almansi strain tensor $\mathbf{e} = \frac{1}{2}(\mathbf{I} - \mathbf{B}^{-1})$. It is not difficult to show that both of these strain measures reduce to the small strain tensor $\boldsymbol{\varepsilon} = \frac{1}{2}(\nabla_X \mathbf{u} + (\nabla_X \mathbf{u})^T)$ if the displacements are sufficiently small.

Another finite strain measure that has gained attention in more recent years is the Hencky (logarithmic, or "true") strain tensor $\mathbf{H} = \frac{1}{2}\log \mathbf{B}$. Because the Hencky strain tensor belongs to the Seth-Hill family of strain measures (as do the Green-Lagrangian and Eulerian-Almansi strain tensors), it likewise is seen to reduce to the small strain tensor in the limit of small displacements.

2.2 Conservation of Linear and Angular Momentum

For a given material body $\mathcal{B}_t \subset \mathbb{R}^d$, any open subset $\Omega_t \subset \mathcal{B}_t$ must satisfy Newton's second law of motion, such that the net external force which acts upon Ω_t is equal to the total change in linear momentum of the system, i.e.

$$\frac{d}{dt}\int_{\Omega_t} \rho \mathbf{v}\, dv = \int_{\Omega_t} \rho \mathbf{b}\, dv + \int_{\partial\Omega_t} \mathbf{t}\, da \quad \forall \Omega_t \subset \mathcal{B}, \tag{2.8}$$

where ρ is the mass density of the matertial, $\mathbf{v}$ is the velocity field, $\mathbf{b}$ is an applied body force per unit of mass, and $\mathbf{t}$ is the traction vector – a force per unit of area – which acts on $\partial\Omega_t$ (the boundary of Ω_t). Via the Cauchy tetrahedron argument, it is possible to express the traction vector $\mathbf{t}(\mathbf{n})$ as a linear function of the unit vector $\mathbf{n}$, which is normal to the surface upon which the traction acts:

$$\mathbf{t} = \mathbf{n} \cdot \boldsymbol{\sigma}, \tag{2.9}$$

where $\boldsymbol{\sigma}$ is referred to as the Cauchy stress tensor. Invoking the divergence theorem, we may utilize the above relation to convert the traction boundary integral into a volume integral over Ω_t:

$$\int_{\partial\Omega_t} \mathbf{t}\, da = \int_{\partial\Omega_t} \mathbf{n} \cdot \boldsymbol{\sigma}\, da = \int_{\Omega_t} \nabla_x \cdot \boldsymbol{\sigma}\, dv. \tag{2.10}$$

Moreover, utilizing Reynolds' transport theorem, conservation of mass, and a change of variables in $\mathbf{x}$ and $\mathbf{X}$, it is possible to show that

$$\frac{d}{dt}\int_{\Omega_t} \rho\mathbf{v}\, dv = \int_{\Omega_t} \rho\frac{d\mathbf{v}}{dt}\, dv, \tag{2.11}$$

which ultimately yields

$$\int_{\Omega_t} \left[\rho(\mathbf{b} - \dot{\mathbf{v}}) + \nabla_x \cdot \boldsymbol{\sigma}\right]\, dv = \mathbf{0} \quad \forall \Omega_t \subset \mathcal{B}. \tag{2.12}$$

Since we have imposed no limitations on the choice of subset Ω_t, we may invoke the localization theorem to determine a point-wise statement of equilibrium in the body $\mathcal{B}_t$:

$$\rho(\mathbf{b} - \dot{\mathbf{v}}) + \nabla_x \cdot \boldsymbol{\sigma} = \mathbf{0} \quad \forall \mathbf{x} \in \mathcal{B}_t. \tag{2.13}$$

Similarly, by formulating an expression for the conservation of angular momentum, we obtain an additional point-wise requirement on the symmetry of the Cauchy stress tensor:

$$\boldsymbol{\sigma} = \boldsymbol{\sigma}^T \quad \forall \mathbf{x} \in \mathcal{B}_t. \tag{2.14}$$

Measures of Stress

As expressed earlier, the Cauchy stress tensor $\boldsymbol{\sigma}$ relates the normal $\mathbf{n}$ of a given surface area element $d\mathbf{a} = \mathbf{n}\, da$ to the corresponding force per unit of area $\mathbf{t}$ which acts on that surface, where the surface element $d\mathbf{a}$ is defined in the current configuration of the body (at some time $t > 0$). The total force which acts on a given surface $d\mathbf{a}$ is then

$$d\mathbf{f} = \mathbf{t}\, da = \boldsymbol{\sigma}^T\, d\mathbf{a}. \tag{2.15}$$

Utilizing Nanson's formula for area transformations:

$$d\mathbf{a} = J\mathbf{F}^{-T}\, d\mathbf{A}, \tag{2.16}$$

we may consider an equivalent representation of $d\mathbf{f}$, such that

$$d\mathbf{f} = J\boldsymbol{\sigma}^T\mathbf{F}^{-T}\, d\mathbf{A} = \mathbf{P}\, d\mathbf{A} = \mathbf{p}\, dA, \tag{2.17}$$

where $\mathbf{P}$ is defined as the first Piola-Kirchhoff stress tensor (which in general is not symmetric.), and where $\mathbf{p} = \mathbf{N} \cdot \mathbf{P}^T$ is the corresponding Piola traction vector, characterizing

the distributed force which acts over a surface defined in the reference configuration with area dA and normal $\mathbf{N}$.

Another stress measure (related to the first Piola-Kirchhoff stress) is the second Piola-Kirchhoff stress tensor $\mathbf{S}$, and is commonly defined as the pull-back of the Kirchhoff stress tensor $\boldsymbol{\tau} = J\boldsymbol{\sigma}$:

$$\mathbf{S} = \mathbf{F}^{-1}\boldsymbol{\tau}\mathbf{F}^{-T}. \tag{2.18}$$

2.3 Constitutive Relations

Fundamentally, we require there to be some relationship between the forces applied to a given body, and its observed deformation. Such relationships are generally referred to as constitutive models, which characterize a macroscopic connection between stress and strain in a continuum.

Models of Elasticity

Constitutive models have variable forms, mostly notably as they relate to notions of elasticity: the tendency of a material to revert to its original undeformed configuration if the applied forces are removed. Models for elastic material behavior fall into three primary categories: hyperelasticity, Cauchy-elasticity, and hypoelasticity.

Hyperelasticity is concerned with the description of a material's state through an elastic potential function, which expresses the total stored elastic strain energy $W(\mathbf{F})$ in the material as a function of the total deformation measured from some (nominally undeformed) reference configuration. Differentiation of this potential with respect to a given deformation measure will yield an expression for the corresponding work-conjugate measure of stress, e.g.

$$\mathbf{P} = \frac{\partial W}{\partial \mathbf{F}}, \qquad \mathbf{S} = \frac{\partial W}{\partial \mathbf{E}}. \tag{2.19}$$

Some common examples of hyperelastic models include the St. Venant-Kirchhoff material model:

$$W(\mathbf{E}) = \frac{\lambda}{2}\mathrm{tr}(\mathbf{E})^2 + \mu\mathrm{tr}(\mathbf{E}^2), \tag{2.20}$$

the Hencky elasticity model:

$$W(\mathbf{H}) = \frac{\lambda}{2}\mathrm{tr}(\mathbf{H})^2 + \mu\mathrm{tr}(\mathbf{H}^2), \tag{2.21}$$

the compressible Mooney-Rivlin solid:

$$W(I_1, I_2, J) = C_{01}(J^{-4/3}I_2 - 3) + C_{10}(J^{-2/3}I_1 - 3) + D_1(J-1)^2, \tag{2.22}$$

$$I_1 = \mathrm{tr}(\mathbf{B}), \qquad I_2 = \frac{1}{2}\left[\mathrm{tr}(\mathbf{B})^2 - \mathrm{tr}(\mathbf{B}^2)\right], \qquad J = \det(\mathbf{F}), \tag{2.23}$$

$$D_1 = \frac{\kappa}{2}, \qquad (C_{01} + C_{10}) = \frac{\mu}{2}, \tag{2.24}$$

and the compressible Neo-Hookean solid (a special case of the Mooney-Rivlin solid where $C_{01} = 0$, and $C_1 = C_{10}$):

$$W(I_1, J) = C_1(J^{-2/3}I_1 - 3) + D_1(J-1)^2 \tag{2.25}$$

Cauchy-elasticity (as a terminology to describe a particular sub-class of material models) differs from hyperelasticity in the sense that the relations between particular stress and strain measures are defined directly, and do not necessarily arise from an elastic potential function. The models of linear elasticity, in particular, are generalizations of Hooke's law, namely:

$$\boldsymbol{\sigma} = \mathbf{C} : \boldsymbol{\varepsilon}, \tag{2.26}$$

and are suitable for small deformations, but are typically not applicable in the context of finite deformations. By comparison, Cauchy-elastic models are defined in terms of the deformation gradient $\mathbf{F}$, i.e.

$$\boldsymbol{\sigma} = f(\mathbf{F}), \tag{2.27}$$

and are suitable in the context of finite deformations. For such models to be considered objective under a superposed rigid rotation corresponding to $\mathbf{R}$, they must satisfy the following condition:

$$\mathbf{R}\boldsymbol{\sigma}\mathbf{R}^T = f(\mathbf{RF}). \tag{2.28}$$

Nonetheless, such models may still suffer from being non-conservative, in the sense that the total work done by the stresses acting on a body moving through an arbitrary closed

cycle of deformation does not necessarily sum to zero. For these reasons, models of hyperelasticity are generally preferred where the use of such models is deemed appropriate. Nonetheless elasticity models are still useful, particularly in the context of small deformations.

In contrast, hypoelasticity models define an evolution (rate) equation in terms of the current stress and the velocity gradient at a given material point, i.e.

$$\dot{\boldsymbol{\sigma}} = g(\boldsymbol{\sigma}, \mathbf{L}). \tag{2.29}$$

Hypoelasticity models are in general non-conservative, and moreover may not necessarily return to a state of zero stress following a closed cycle of deformation. Hypoelasticity is generally less appropriate where hyperelastic or other elastic models may be used instead. The value of hypoelasticity lies in its ability to accomodate models for plastic flow and dissipation in the material, giving rise to the common models of hypoelasto-plasticity.

One of the primary challenges of working with hypoelastic models concerns the manner in which the rate of stress transforms under superposed rigid-body rotations. These considerations have led to the formulation of co-rotational (or objective) stress rates. A multitude of such rates exist, though only a few are found to be in common usage. Most notably, the Jaumann rate of stress $\mathring{\boldsymbol{\sigma}}$ is defined as

$$\mathring{\boldsymbol{\sigma}} = g(\boldsymbol{\sigma}, \mathbf{D}) = \dot{\boldsymbol{\sigma}} + \boldsymbol{\sigma}\mathbf{W} - \mathbf{W}\boldsymbol{\sigma}, \tag{2.30}$$

where $\mathbf{D}$ and $\mathbf{W}$ specify the rate of deformation and spin at a given material point, respectively.

2.4 Model Boundary Value Problem

Up to this point, we have discussed only the essential relationships which exist between physical quantities of interest in the context of solid mechanics. Ultimately, however, we should like to determine the anticipated motion and deformation of a particular body under the action of pre-determined externally applied forces. To this end, we must turn our attention to the definition – and solution – of boundary value problems (BVPs). Such problems must be well-posed, in the sense that there exists a unique solution to the stated problem, thereby imposing certain restrictions on the choice of boundary conditions.

The Strong Form Statement of Equilibrium

In the context of solid mechanics, the solution of a given boundary value problem usually refers to a complete description of the primary field variable(s) of interest, namely the displacement field $\mathbf{u}(\mathbf{X})$ at all locations $\mathbf{X} \in \mathcal{B}_0$ within the body $\mathcal{B}_0$ in its reference configuration. Under the requirements of compatibility, we presume that the displacement field is a continuous function, whose derivatives up to second order are defined everywhere, i.e. $\mathbf{u} \in [C^2(\mathcal{B}_0)]^d$.

Now, let us examine a quasi-static solid mechanics model problem of the following form: consider an open domain $\mathcal{B}_0 \subset \mathbb{R}^d$ whose boundary $\partial\mathcal{B}_0$ consists of the partition $\left\{\Gamma_0^D, \Gamma_0^N\right\}$. Let $\mathbf{u} = \bar{\mathbf{u}}\ \forall \mathbf{X} \in \Gamma_0^D$ constitute a prescribed Dirichlet boundary condition imposed upon the displacement field, and $\mathbf{n} \cdot \boldsymbol{\sigma} = \bar{\mathbf{t}}\ \forall \mathbf{X} \in \Gamma_0^N$ be a Neumann boundary condition imposed upon the surface traction. Additionally, let us suppose that an applied body force $\mathbf{b}$ acts upon all points $\mathbf{X} \in \mathcal{B}_0$. Given these conditions, we should like to determine the displacement field $\mathbf{u} \in \mathcal{S} = \left\{\mathbf{u} \in [C^2(\mathcal{B}_0)]^d : \mathbf{u} = \bar{\mathbf{u}}\ \forall \mathbf{x} \in \Gamma_0^D\right\}$ which satisfies the equations of equilibrium in a point-wise sense:

$$\rho\mathbf{b} + \nabla_x \cdot \boldsymbol{\sigma} = \mathbf{0} \quad \forall \mathbf{x} \in \mathcal{B}_t, \tag{2.31}$$

and where we suppose that a constitutive model has been defined in order to relate some measure of the deformation (e.g. $\mathbf{F} = \mathbf{1} + \nabla_X \mathbf{u}$) to the stress (e.g. $\boldsymbol{\sigma} = f(\mathbf{F})$). Equivalently, we may write the equations of equilibrium in terms of quantities related to the reference configuration of the body:

$$\rho_0\mathbf{b} + \nabla_X \cdot \mathbf{P}^T = \mathbf{0} \quad \forall \mathbf{X} \in \mathcal{B}_0, \tag{2.32}$$

where $\rho_0 = J\rho$ is the mass density of the material at time $t = 0$. The above statement is commonly referred to as the "strong form" of the model problem, given that it requires a point-wise satisfaction of equilibrium.

It should be emphasized that the Dirichlet boundary conditions and the requirements of compatibility are satisfied implicitly, as a consequence of the deliberate choice of function space $\mathcal{S}$ for the displacement field. Such functions $\mathbf{u} \in \mathcal{S}$ are termed "admissible," as potential solutions to the boundary value problem at hand.

The Equivalent Weak Form Statement of Equilibrium

In general, solutions to the strong form problem are not easily obtained. For this reason, it proves to be much more convenient to work with the (equivalent) "weak form" statement of the boundary value problem:

Find $\mathbf{u} \in \mathcal{S} = \left\{ \mathbf{u} \in [H^1(\mathcal{B}_0)]^d : \mathbf{u} = \bar{\mathbf{u}} \ \forall \mathbf{X} \in \Gamma_0^D \right\}$ *such that*

$$\mathcal{R}(\mathbf{u}, \mathbf{v}) = \int_{\mathcal{B}_t} \rho \mathbf{b} \cdot \mathbf{v} \, dv + \int_{\Gamma_t^N} \bar{\mathbf{t}} \cdot \mathbf{v} \, da - \int_{\mathcal{B}_t} \boldsymbol{\sigma} \colon \nabla_x \mathbf{v} \, dv = 0 \quad \forall \mathbf{v} \in \mathcal{V}, \tag{2.33}$$

or equivalently

$$\mathcal{R}(\mathbf{u}, \mathbf{v}) = \int_{\mathcal{B}_0} \rho_0 \mathbf{b} \cdot \mathbf{v} \, dV + \int_{\Gamma_0^N} \bar{\mathbf{p}} \cdot \mathbf{v} \, dA - \int_{\mathcal{B}_0} \mathbf{P} \colon \nabla_X \mathbf{v} \, dV = 0 \quad \forall \mathbf{v} \in \mathcal{V}, \tag{2.34}$$

where $\mathcal{V} = \left\{ \mathbf{v} \in [H^1(\mathcal{B}_0)]^d : \mathbf{v} = \mathbf{0} \ \forall \mathbf{X} \in \Gamma_0^D \right\}$, *and*

$$H^1(\mathcal{B}_0) = \left\{ u \in L^2(\mathcal{B}_0), \, D^\alpha u \in L^2(\mathcal{B}_0) \ \forall |\alpha| \leq 1 \right\}. \tag{2.35}$$

It should be remarked that the space $\mathcal{S}$ of admissible solutions to the weak form now consists of much more general functions than those considered for the strong form. In other words, the requirements on the differentiability of functions in $\mathcal{S}$ have been "weakened."

In (2.34), the traction boundary condition has been replaced by $\mathbf{p} = \bar{\mathbf{p}} \ \forall \mathbf{X} \in \Gamma_0^N$ – i.e. a condition on the Piola (rather than Cauchy) surface traction. The function space $\mathcal{S}$ is commonly referred to as the space of admissible "trial solutions," whereas $\mathcal{V}$ is called the space of "test functions," and consists of all admissible variations such that $\mathcal{V} = T_{\mathbf{u}}\mathcal{S}$ is the tangent space to $\mathcal{S}$ (i.e. $\mathbf{u} + \mathbf{v} \in \mathcal{S} \ \forall \mathbf{u} \in \mathcal{S}, \, \mathbf{v} \in \mathcal{V}$). In words, our goal is determine the solution $\mathbf{u}$ from among all admissible trial solutions contained in $\mathcal{S}$ which satisfies equation (2.33) or (2.34) for all admissible variations $\mathbf{v} \in \mathcal{V}$.

Under the assumptions of small displacements and linear elasticity, equations (2.33) and (2.34) are equivalent, and may be more succinctly expressed in terms of a bilinear form $a \colon \mathcal{S} \times \mathcal{V} \mapsto \mathbb{R}$ and a linear form $\ell : \mathcal{V} \mapsto \mathbb{R}$ such that

$$a(\mathbf{u}, \mathbf{v}) + \ell(\mathbf{v}) = 0 \quad \forall \mathbf{v} \in \mathcal{V}. \tag{2.36}$$

2.5 Galerkin Approximations to the Weak Form

In the weak form problem statement, the trial and test spaces $\mathcal{S}$ and $\mathcal{V}$ are taken to be infinite dimensional function spaces. In a practical computational setting, however, this renders the solution of such problems infeasible. Instead, most variational methods consider approximate solutions to the weak form, where $\mathbf{u} \in \mathcal{S}$ and $\mathbf{v} \in \mathcal{V}$ are replaced by $\mathbf{u}^h \in \mathcal{S}^h \subset \mathcal{S}$ and $\mathbf{v}^h \in \mathcal{V}^h \subset \mathcal{V}$, respectively. In this context, $\{\varphi_a\}_{a=1}^N$ and $\{\phi_a\}_{a=1}^M$ denote finite dimensional bases for the sub-spaces $\mathcal{S}^h$ and $\mathcal{V}^h$, such that

$$\mathbf{u}^h(\mathbf{X}) = \sum_{a=1}^{N} \varphi_a(\mathbf{X})\mathbf{u}_a, \qquad \mathbf{v}^h(\mathbf{X}) = \sum_{a=1}^{M} \phi_a(\mathbf{X})\mathbf{v}_a. \tag{2.37}$$

This yields the Galerkin approximation to the weak form: *Find* $\mathbf{u}^h \in \mathcal{S}^h$ *such that*

$$\mathcal{R}(\mathbf{u}^h, \mathbf{v}^h) = 0 \quad \forall \mathbf{v}^h \in \mathcal{V}^h, \tag{2.38}$$

yielding the (in general, nonlinear) residual equations, in index notation:

$$R_{ia}(\mathbf{u}^h) = \int_{\mathcal{B}_0} \rho_0 b_i \phi_a \, dV + \int_{\Gamma_0^N} \bar{p}_i \phi_a \, dA - \int_{\mathcal{B}_0} P_{ij} \phi_{a,j} \, dV = 0 \quad \forall i,\, a. \tag{2.39}$$

Without loss of generality, if we suppose that $\mathcal{S} = \mathcal{V}$ (provided $\mathbf{u} = \mathbf{0}\ \forall \mathbf{X} \in \Gamma_0^D$), then we may select identical sub-spaces $\mathcal{S}^h = \mathcal{V}^h$ ($\{\varphi_a\}_{a=1}^N = \{\phi_a\}_{a=1}^M$), resulting in a symmetric (or Bubnov-) Galerkin method. Traditional finite element methods fall into this category. Such methods are advantageous in the sense that (for linear problems) they result in stable, symmetric bilinear forms satisfying the Galerkin orthgonality (or "best approximation") property – the property that the solution error $\mathbf{e} = \mathbf{u}^h - \mathbf{u}$ is orthogonal to the chosen sub-space $\mathcal{S}^h$.

Petrov-Galerkin methods consider the more general case where $\mathcal{V}^h \neq \mathcal{S}^h$, resulting in differing trial and test function spaces. Such methods must guarantee satisfaction of the LBB (inf-sup) conditions to achieve convergence. Consequently, the selection of appropriate trial and test function spaces which result in stable discretizations is not trivial. Nonetheless, Petrov-Galerkin methods allow for greater flexibility in the construction of numerical approximation schemes.

Finite Element Methods

Finite element methods (FEM) are predicated on the idea that a problem domain $\mathcal{B}_0$ can be discretized into a finite number of simpler sub-domains $\Omega_e \subset \mathcal{B}_0$, individually called elements, and collectively referred to as a "mesh." The basis functions are assumed to be low-order polynomials within each element, and are compactly supported over a given patch of elements. The traditional finite element method assumes these basis functions to be C^0 continuous at element boundaries, yielding a priori satisfaction of compatibility.

Individual FE basis functions φ_a are typically associated with the "nodes" $\mathbf{X}_a$ of the mesh (located at element verticies, along element edges, etc.), such that the kronecker delta property is satisfied, i.e. $\varphi_a(\mathbf{X}_b) = \delta_{ab}$. Consequently, the basis functions comprise a set of interpolants for discrete values of the solution defined at the nodes.

Elements consisting of regular shapes (tetrahedra, hexahedra) also provide a natural means of effecting numerical integration of the weak form through the use of the isoparametric transformation and product Gaussian quadrature rules.

Consistent Linearization of the Weak Form

In order to determine the solution $\mathbf{u}^h \in \mathcal{S}^h$ satisfying the weak form equations, we will choose to employ a Newton-Raphson algorithm:

Compute initial guess $u_{jb}^{(0)}$;
while $||R_{ia}|| < \epsilon$ **do**
  Assemble $K_{iajb} = \partial R_{ia}/\partial u_{jb}$;
  Update $u_{jb}^{(k+1)} \leftarrow u_{jb}^{(k)} - K_{jbia}^{-1} R_{ia}$;
end

Algorithm 1: Newton-Raphson Iteration

Here, R_{ia} denotes the residual (vector), and K_{iajb} denotes the stiffness matrix – the Jacobian of the residual with respect to the independent unknowns u_{jb} (the nodal displacements). The above iteration procedure is repeated until the stopping criterion $||R_{ia}|| < \epsilon$ is reached, for some specified residual measure $||\cdot||$, and tolerance ϵ.

Given the residual equations $R_{ia}(\mathbf{u}^h) = 0 \, \forall i, a$, we may express their first partial

derivatives $\partial R_{ia}/\partial u_{jb}$ with respect to the independent unknowns u_{jb} as

$$\frac{\partial R_{ia}}{\partial u_{jb}} = \int_{\Gamma_0^N} \frac{\partial \bar{p}_i}{\partial u_{jb}} \phi_a \, dA - \int_{\mathcal{B}_0} \frac{\partial P_{ik}}{\partial u_{jb}} \phi_{a,k} \, dV, \tag{2.40}$$

indicating two primary terms ($\bar{\mathbf{p}}$ and $\mathbf{P}$) which must be linearized. Subsequent discussions will focus on the linearization of the first Piola-Kirchhoff stress.

Nonlinear Deformation and Incremental Kinematics

Let us contemplate the linearization of $\partial P_{ik}/\partial u_{jb}$ by applying the chain-rule:

$$\frac{\partial P_{ik}}{\partial u_{jb}} = \frac{\partial P_{ik}}{\partial F_{lm}} \frac{\partial F_{lm}}{\partial u_{jb}}, \tag{2.41}$$

revealing the deformation "gradient operator:"

$$\frac{\partial F_{lm}}{\partial u_{jb}} = \delta_{jl} \varphi_{b,m}. \tag{2.42}$$

If a enhanced strain formulation is employed, only the gradient operator would need to be modified; the subsequent expressions pertaining to $\partial P_{ik}/\partial F_{lm}$ would remain unchanged.

Through further application of the chain-rule, and use of the following identities:

$$\frac{\partial J}{\partial F_{lm}} = J F^{-1}_{ml}, \quad \frac{\partial F^{-1}_{kj}}{\partial F_{lm}} = F^{-1}_{kl} F^{-1}_{mj}, \tag{2.43}$$

one can derive the following result:

$$\frac{\partial P_{ik}}{\partial F_{lm}} = J \sigma_{ij} (F^{-1}_{ml} F^{-1}_{kj} + F^{-1}_{kl} F^{-1}_{mj}) + J \frac{\partial \sigma_{ij}}{\partial F_{lm}} F^{-1}_{kj}. \tag{2.44}$$

If the material model allows for the Cauchy stress to be written directly as a function of the deformation gradient (i.e. $\boldsymbol{\sigma} = f(\mathbf{F})$, as is the case for Cauchy-elastic material models), then a consistent linearization for $\partial \sigma_{ij}/\partial F_{lm}$ may be obtained by direct differentiation.

Otherwise (for hypoelastic material models of the form $\dot{\boldsymbol{\sigma}} = g(\boldsymbol{\sigma}, \mathbf{L})$), we must consider the integral of the stress rate over some finite time interval $\Delta t = t_{k+1} - t_k$:

$$\boldsymbol{\sigma}_{k+1} = \boldsymbol{\sigma}_k + \int_{t_k}^{t_{k+1}} \dot{\boldsymbol{\sigma}} \, dt. \tag{2.45}$$

The corresponding increment of motion is characterized by $\hat{\mathbf{F}} = \mathbf{F}_{k+1} \mathbf{F}_k^{-1} = \hat{\mathbf{R}} \hat{\mathbf{U}}$, which is used to update the stress via the following incremental algorithm (proposed in [33]):

$$\boldsymbol{\sigma}_{k+1} = \hat{\mathbf{R}} \left[\boldsymbol{\sigma}_k + \int_{t_k}^{t_{k+1}} \mathring{\boldsymbol{\sigma}}(\mathbf{D}) \, dt \right] \hat{\mathbf{R}}^T, \tag{2.46}$$

where $\mathbf{D} = \frac{1}{\Delta t}\log\hat{\mathbf{U}}$ denotes the time-averaged rate of deformation over the time step. The resulting algorithmically consistent tangent $\partial\sigma_{ij}/\partial F_{lm}$ is computed as

$$\frac{\partial\sigma_{ij}}{\partial F_{lm}} = \frac{\partial\hat{R}_{ik}}{\partial F_{lm}}\hat{R}_{nk}\sigma_{nj} + \sigma_{in}\hat{R}_{nk}\frac{\partial\hat{R}_{jk}}{\partial F_{lm}} + \hat{R}_{ik}C_{knpq}\hat{R}_{jn}\frac{\partial D_{pq}}{\partial F_{lm}}\Delta t, \tag{2.47}$$

where $C_{knpq} \equiv \partial\mathring{\sigma}_{kn}/\partial D_{pq}$ (the material tangent modulus) is supplied by the constitutive model. The computation of $\partial\hat{R}_{ik}/\partial F_{lm}$ and $\partial D_{pq}/\partial F_{lm}$ may be accurately carried out with the aid of the following expressions:

$$\frac{\partial\hat{D}_{pq}}{\partial\hat{U}_{ij}} = \frac{1}{\Delta t}\sum_{r,s}\hat{Q}_{qr}\hat{Q}_{jr}\mathcal{H}(f,\hat{\lambda}_r,\hat{\lambda}_s)\hat{Q}_{ps}\hat{Q}_{is}; \quad f(\lambda) = \log(\lambda), \tag{2.48}$$

$$\frac{\partial\hat{U}_{ij}}{\partial\hat{B}_{kl}} = \sum_{r,s}\hat{Q}_{jr}\hat{Q}_{lr}\mathcal{H}(g,\hat{\lambda}_r^2,\hat{\lambda}_s^2)\hat{Q}_{is}\hat{Q}_{ks}; \quad g(\lambda) = \sqrt{\lambda}, \tag{2.49}$$

$$\frac{\partial\hat{B}_{kj}}{\partial F_{lm}} = F^{-1}_{mi}(\hat{F}_{ik}\hat{F}_{lj} + \hat{F}_{ij}\hat{F}_{lk}), \tag{2.50}$$

$$\frac{\partial\hat{R}_{ik}}{\partial F_{lm}} = \delta_{il}\hat{R}_{mj}F^{-1}_{jk} - \hat{R}_{in}\frac{\partial\hat{U}_{nj}}{\partial F_{lm}}\hat{U}^{-1}_{jk}, \tag{2.51}$$

where we define

$$\mathcal{H}(f,x,y) \equiv \begin{cases} f'(x), & x = y \\ \frac{f(x)-f(y)}{x-y} & x \neq y \end{cases}, \tag{2.52}$$

and $\hat{\mathbf{U}} = \hat{\mathbf{Q}}\hat{\mathbf{\Lambda}}\hat{\mathbf{Q}}^T$ represents the eigendecomposition of $\hat{\mathbf{U}}$, and $\hat{\lambda}_i$ denote the corresponding eigenvalues of $\hat{\mathbf{U}}$.

2.6 Requirements for Convergence of an Approximation Method

Because variational methods utilize finite dimensional spaces $\mathcal{S}^h$ and $\mathcal{V}^h$, they inherrently incur some error $\mathbf{e} = \mathbf{u}^h - \mathbf{u}$ in approximating the exact solution to the original boundary value problem. The approximation power of a given method is typically characterized by the rate at which a specified error measure $||\mathbf{u}^h - \mathbf{u}||$ (defined on $\mathcal{S}$) decreases as the dimension N of the approximation space $\mathcal{S}^h$ is systematically increased. For finite element methods, increasing the dimension N of the approximation space is synonymous with refining the discretization, to the extent that a specified mesh parameter h (the

diameter of the largest element in the mesh) is decreased. An approximation method will therefore yield solutions $\mathbf{u}^h$ which converge to the exact solution $\mathbf{u}$, provided

$$\lim_{N\to\infty} ||\mathbf{u}^h - \mathbf{u}|| = \lim_{h\to 0} ||\mathbf{u}^h - \mathbf{u}|| = 0. \tag{2.53}$$

Further, a method whose solution error can be bounded by an estimate

$$||\mathbf{u}^h - \mathbf{u}|| \leq Ch^\alpha ||\mathbf{u}||, \tag{2.54}$$

will converge at a rate of order α.

For an approximation method to achieve convergence, several conditions must be satisfied, namely: approximability, compatibility, stability, and quadrature consistency. These conditions are summarized in the following sections.

Approximability

To achieve α^{th}-order convergence, the approximation space $\mathcal{S}^h$ must contain $[P^k(\mathcal{B}_0)]^d$ (the space of vector-valued polynomial functions of maximal degree $k = \alpha + 1$) as a subset $\mathcal{S}^h \supset [P^k(\mathcal{B}_0)]^d$.

This property is sometimes referred to as *approximability*, reflecting a given method's ability to well-approximate the solution locally as a low-order polynomial. Alternativley, this condition is known as polynomial *reproducibility*, or *completeness*. This condition can be rationalized by the Weierstrass approximation theorem, which asserts that any smooth function can be approximated by polynomials to arbitrary precision.

Compatibility

Compatibility, in an abstract sense, imposes requirements upon the continuity of trial solutions $\mathbf{u}^h \in \mathcal{S}^h$. For conforming finite element methods, this condition is automatically satisfied, as the trial solution space consists of sufficiently continuous functions, such that $\mathcal{S}^h \subset C^0$.

By comparison, non-conforming finite element methods admit more general functions $\mathbf{u}^h \in \mathcal{S}^h \not\subset C^0$. Such spaces of functions must satisfy additional weak compatibility requirements. Namely, Stummel has proposed in [42] the necessary and sufficient conditions

for convergence of a non-conforming finite element method, necessitating passage of the *generalized patch test*:

For a given patch $\mathcal{P} \subset \overline{\mathcal{B}}_0$ and an approximating sequence of functions $u^h \in H^k(\mathcal{B}_0)$: for every $\mathbf{X} \in \mathcal{P}$ there exists an open neighborhood O in $\mathbb{R}^d$ such that

$$\lim_{h\to 0} \sum_{\forall \Omega_e} \int_{\partial\Omega_e} v\, D^\alpha u^h|_{\Omega_e} \mathbf{n}\, da = \mathbf{0} \tag{2.55}$$

for all test functions $v \in C_0^\infty(O)$, and $|\alpha| \leq k-1$.

Shi later proposed the F-E-M test in [10] as an alternative, sufficient condition for convergence, with a corresponding interface requirement (the F-test):

$$\left| \int_{\Omega_a \cap \Omega_b} [\![u^h]\!]\, da \right| \leq O(h^{d/2}) ||u^h||_{\Omega_a \cup \Omega_b} \quad \forall \Omega_a \cap \Omega_b \neq \emptyset. \tag{2.56}$$

Stability

The LBB (inf-sup) conditions (introduced in [1], [5]) pertain to potentially differing choices for $\mathcal{S}^h$ and $\mathcal{V}^h$ with appropriately defined norms. For the model problem with bilinear form $a\colon \mathcal{S} \times \mathcal{V} \to \mathbb{R}$, *uniqueness* of a given solution is contingent upon the inf-sup condition:

$$\inf_{u^h \in \mathcal{S}^h} \sup_{v^h \in \mathcal{V}^h} \frac{a(u^h, v^h)}{||u^h||\, ||v^h||} > 0. \tag{2.57}$$

If a is symmetric and $\mathcal{S}^h = \mathcal{V}^h$, this condition is equivalent to the requirement that a be ellipitic (coercive):

$$a(u^h, u^h) \geq C_c ||u^h||^2 \quad \forall u^h \in \mathcal{S}^h. \tag{2.58}$$

Existence of a solution further depends upon the condition that a be bounded:

$$a(u^h, v^h) \leq C_b ||u^h||\, ||v^h|| \quad \forall u^h \in \mathcal{S}^h,\, v^h \in \mathcal{V}^h, \tag{2.59}$$

and surjective:

$$\sup_{u^h \in \mathcal{S}^h} a(u^h, v^h) > 0 \quad \forall v^h \in \mathcal{V}^h. \tag{2.60}$$

Heuristically, these conditions require that individual element stiffness matricies be of full rank, excluding rigid body modes of deformation. This necessitates both: the specification of a stable discretization, and sufficiently accurate evaluation (numerical integration) of the weak form.

Quadrature Consistency

Considering the variational formulation of the model boundary value problem in (2.34), if the exact solution $\mathbf{u} \in \mathcal{S}$ to the weak form is contained within the chosen approximation space (i.e. if $\mathbf{u} \in \mathcal{S}^h$), we require that $\mathbf{u}$ be identified as the unique solution to the Galerkin approximation in (2.38), namely:

$$\mathcal{R}(\mathbf{u}, \mathbf{v}^h) = 0 \quad \forall \mathbf{v}^h \in \mathcal{V}^h. \tag{2.61}$$

This property is referred to as *Galerkin exactness*, and is particularly relevant to the satisfaction of finite element patch tests, which demonstrate Galerkin exactness when the exact solution is a low-order polynomial.

In particular, given a stress field $P_{ij}(\mathbf{u})$ arising from the exact solution $\mathbf{u} \in \mathcal{S}^h$, and for the given boundary conditions $\bar{p}_i = P_{ij}N_j$ and $\rho_0 b_i = -P_{ij,j}$, we may express the residual equations as

$$R_{ia} = \int_{\mathcal{B}_0} P_{ij}\phi_{a,j}\, dV + \int_{\mathcal{B}_0} P_{ij,j}\phi_a\, dV - \int_{\partial\mathcal{B}_0} P_{ij}N_j\phi_a\, dA = 0 \quad \forall i,\, a. \tag{2.62}$$

If we suppose that the exact solution is well-approximated by low-order polynomials, i.e.

$$u_i(\mathbf{X}) = \sum_{|\alpha|=0}^{k} a_{i\alpha}\mathbf{X}^\alpha, \quad P_{ij}(\mathbf{X}) = \sum_{|\alpha|=0}^{k-1} b_{ij\alpha}\mathbf{X}^\alpha, \tag{2.63}$$

then the resulting conditions for Galerkin exactness are:

$$\int_{\mathcal{B}_0} \mathbf{X}^\alpha \phi_{a,i}\, dV + \int_{\mathcal{B}_0} \mathbf{X}^\alpha_{,i}\phi_a\, dV = \int_{\partial\mathcal{B}_0} \mathbf{X}^\alpha N_i\phi_a\, dA \quad \forall i,\, a,\, |\alpha| \leq k-1. \tag{2.64}$$

The above consistency requirements are required to hold over the problem domain $\mathcal{B}_0$ as a whole, or equivalently over each individual element domain Ω_e:

$$\int_{\Omega_e} \mathbf{X}^\alpha \phi_{a,i}\, dV + \int_{\Omega_e} \mathbf{X}^\alpha_{,i}\phi_a\, dV = \int_{\partial\Omega_e} \mathbf{X}^\alpha N_i\phi_a\, dA \quad \forall i,\, a,\, |\alpha| \leq k-1,\, \Omega_e \subset \mathcal{B}_0. \tag{2.65}$$

The above conditions are sufficient for satisfaction of the Irons patch test up to k^{th} order, provided $\mathcal{S}^h \supset [P^k(\mathcal{B}_0)]^d$. It should be emphasized that these conditions apply specifically to the test functions $\phi_a \in \mathcal{V}^h$.

In most practical situations, however, the integral expressions in (2.38) are evaluated only approximately; numerical quadrature rules are defined on the elements and on their boundaries, such that

$$\int_{\Omega_e} f(\mathbf{X})dV \approx \sum_{q=1}^{N_q} w_q f(\mathbf{X}_q), \quad \int_{\partial\Omega_e} f(\mathbf{X})dA \approx \sum_{b=1}^{N_b} w_b f(\mathbf{X}_b). \tag{2.66}$$

This yields a discrete form of (2.65), henceforth referred to as *quadrature consistency*:

$$\sum_{q=1}^{N_q} w_q \left[\mathbf{X}_q^\alpha \phi_{a,i}^{(q)} + \mathbf{X}_{q,i}^\alpha \phi_a^{(q)} \right] = \sum_{b=1}^{N_b} w_b \mathbf{X}_b^\alpha N_i^{(b)} \phi_a^{(b)} \quad \forall i,\, a,\, |\alpha| \leq k-1,\, \Omega_e \subset \mathcal{B}_0. \tag{2.67}$$

These conditions effectively impose a set constraints on the accuracy of the chosen quadrature rules, and/or on the choice of test functions. Failure to satisfy the above conditions results in issues of integration error, and correspondingly, loss of convergence.

Chapter 3

Partitioned Element Methods

This chapter defines a general class of polytopal element formulations referred to as partitioned element methods (PEM). The essential characteristics and mathematical requirements placed upon these methods are formally stated, giving rise to a family of different approaches, for which some formal investigations are conducted. Several specific formulations are summarized in detail, and a number of existing methods are herein classified as particular instances of partitioned element methods.

3.1 Overview

Partitioned element methods are finite element-like methods which approach the task of constructing shape functions on arbitrary polytopal element domains by partitioning each element into sub-domains (quadrature cells). The element partition serves a dual purpose: it is used to establish a composite quadrature rule for the element, and to define a finite dimensional function space, from which the element's shape functions are selected as the solutions to corresponding boundary value problems defined locally on the element.

Partitioned element methods are motivated by the idea that it is generally easier and more efficient to define complicated functions over arbitrary domains if the functions are defined in a piece-wise polynomial fashion over simpler sub-domains. This is precisely the mentality which likewise motivates the finite element method. The PEM is driven by the need for establishing stable and efficient quadrature rules on arbitrary polytopes. Unlike virtual element methods which typically circumvent the use of quadrature altogether,

partitioned element methods recognize the necessity of using domain quadrature rules to evaluate nonlinear residual and stiffness contributions. The use of sufficient quadrature also yields a stable integration of the weak form which does not rely upon unphysical stabilization parameters.

In contrast with most traditional perspectives which regard the shape functions as being continuously defined on element domains (i.e. generalized barycentric coordinates), the PEM exploits the fact that the shape functions and their gradients only need to be evaluated at a discrete number of quadrature points. With this in mind, PEM approximation spaces are deliberately centered around the quadrature cell partition of the element, and consequently resemble finite element approximation spaces.

The resulting shape functions on each element are altogether subject to the conditions of approximability, compatibility, stability, and quadrature consistency, as discussed in chapter 2. Together, these conditions impose a number of unique requirements upon the element's partition, it's corresponding quadrature rules, and the associated cell-based approximation spaces.

In the following sections, an abstract framework for the PEM is established, describing the corresponding shape function boundary value problems defined on an element. We further enumerate several specific partitioned element methods, and provide an assessment of their potential strengths and weaknesses.

3.2 Definition of Element Shape Functions

Consider the structure of a polyhedral element $\Omega \subset \mathbb{R}^3$, as depicted in figure (N). The element's boundary $\partial\Omega$ may be subdivided into a set of polygonal faces $\mathcal{T}_F(\Omega) = \{F_i\}_{i=1}^{N_F}$, such that each face F_i is shared entirely with an adjacent element, or with the mesh boundary. Corresponding sets of linear edges $\mathcal{T}_E(\Omega) = \{E_i\}_{i=1}^{N_E}$ and nodes $\mathcal{T}_V(\Omega) = \{V_i\}_{i=1}^{N_V}$ result by considering the sets of all unique intersections $\mathcal{T}_E(\Omega) = \{F_i \cap F_j \neq \emptyset \ \forall i \neq j\}$ and $\mathcal{T}_V(\Omega) = \{E_i \cap E_j \neq \emptyset \ \forall i \neq j\}$, respectively.

The function spaces under consideration in the PEM are effectively broken $H^k(\Omega)$ spaces, where a given function $u \in \mathcal{W}_k(\overline{\Omega})$ is defined independently on the open interior

of each polyhedral element $\Omega \subset \mathbb{R}^3$, and on its boundary $\partial\Omega$, such that

$$\mathcal{W}_k(\overline{\Omega}) = \left\{ u|_\Omega \in H^k(\Omega) : \mathcal{L}_\Omega u = f_\Omega \,\text{in}\, \Omega,\, u|_F \in \mathcal{W}_k(\overline{F})\ \forall F \in \partial\Omega \right\}, \tag{3.1}$$

$$\mathcal{W}_k(\overline{F}) = \left\{ u|_F \in H^k(F) : \mathcal{L}_F u = f_F \,\text{in}\, F,\, u|_E \in \mathcal{W}_k(\overline{E})\ \forall E \in \partial F \right\}, \tag{3.2}$$

$$\mathcal{W}_k(\overline{E}) = \left\{ u|_E \in H^k(E) : \mathcal{L}_E u = f_E \,\text{in}\, E,\, u|_V \in \mathbb{R}\ \forall V \in \partial E \right\}. \tag{3.3}$$

In essence, the PEM supposes that a given function $u|_\Omega \in H^k(\Omega)$ defined on the element's interior is related to a corresponding boundary function $u|_{\partial\Omega} = \bar{u}$ (which itself is a broken $H^k(\partial\Omega)$ function) via a well-posed Dirichlet boundary value problem:

$$\mathcal{L}_\Omega u = f_\Omega \quad \forall \mathbf{X} \in \Omega \quad \text{s.t.} \quad u = \bar{u} \quad \forall \mathbf{X} \in \partial\Omega, \tag{3.4}$$

where $\mathcal{L}_\Omega$ denotes a linear differential operator, and $f_\Omega \in L^2(\Omega)$ is a generic forcing function. The element's degrees of freedom are collectively accounted for in both $\bar{u}$ and f_Ω. Consequently, the interior function $u|_\Omega$ is uniquely defined, provided there exists a unique solution to (3.4). In turn, we suppose that $u|_F \in H^k(F)$ is the solution to a similar (2-dimensional) boundary value problem defined on each face F, and $u|_E \in H^k(E)$ is the solution to a (1-dimensional) BVP on each edge E.

The advantage of defining shape functions in this manner is that it affords a great deal of flexibility in the construction of arbitrary order interpolants, while maintaining C^0 continuity at inter-element interfaces. Moreover, given that the shape functions are uniquely defined at every point $\mathbf{X} \in \Omega$, they are amenable to post-processing and visualization-related tasks.

Harmonic Shape Functions

The simplest choice of $\mathcal{L}_\Omega = -\nabla^2$ and $f_\Omega = 0$ corresponds to Laplace's equation:

$$\nabla^2 u = 0 \quad \forall \mathbf{X} \in \Omega \quad \text{s.t.} \quad u = \bar{u} \quad \forall \mathbf{X} \in \partial\Omega, \tag{3.5}$$

whose solution u is harmonic on Ω. Harmonic shape functions form a partition of unity, are linearly complete, and arise from degrees of freedom $u|_V$ borne only by the nodes of each element (therefore, they satisfy the kronecker delta property.) As such, harmonic shape functions are classifiable under the category of generalized barycentric coordinates.

If instead $f_\Omega \neq 0$ (corresponding to Poisson's equation), then

$$-\nabla^2 u = f_\Omega \quad \forall \mathbf{X} \in \Omega \quad \text{s.t.} \quad u = \bar{u} \quad \forall \mathbf{X} \in \partial\Omega, \tag{3.6}$$

and we may introduce additional degrees of freedom through f_Ω belonging to edges, faces, or element domains. These degrees of freedom are not necessarily associated with nodal evaluations of u, but instead may be designed to exhibit certain desirable characteristics. The solution u to (3.6) is not harmonic; instead, we shall refer to such functions as *generalized harmonic shape functions*.

Harmonic shape functions are not a new concept; Gordon and Wixom were among the first authors to propose the idea in [21], and Martin et al. later considered their application to polyhedral finite elements in [28]. However, obtaining exact solutions to (3.5) is generally infeasible for arbitrary polyhedra. In practice, approximate solutions must be considered.

In particular, Bishop has proposed a method for constructing FE approximations to harmonic shape functions in [4]. Additionally, the VETFEM ([34], [36]) and the original PEM presented in [35], may be viewed as techniques for obtaining discrete approximations to harmonic shape functions. Likewise, many virtual element methods ([7], [11], [12]) suppose that the element shape functions are harmonic over individual element domains, though they are never explicitly constructed or represented as such.

It herein becomes of interest to determine suitable approximations to harmonic shape functions on arbitrary polyhedra. A number of methods to achieve this end are discussed in the following section.

Shape Function Approximation Methods

The exact solution $u_0 \in \mathcal{S}(\Omega) = \{u \in H^1(\Omega) : u = u_b \, \forall \mathbf{X} \in \partial\Omega\}$ to the more general Poisson equation in (3.6) satisfies the equivalent weak form:

$$\int_\Omega (\nabla^2 u_0 + f) v_0 \, dV = 0 \quad \forall v_0 \in \mathcal{V}(\Omega), \tag{3.7}$$

or equivalently

$$\int_\Omega \nabla u_0 \cdot \nabla v_0 \, dV - \int_{\partial\Omega} \frac{\partial u_0}{\partial N} v_0 \, dA = \int_\Omega f v_0 \, dV \quad \forall v_0 \in \mathcal{V}(\Omega), \tag{3.8}$$

where $\mathcal{V}(\Omega) = \{v \in H^1(\Omega) : v = 0 \, \forall \mathbf{X} \in \partial\Omega\}$ denotes an appropriately defined space of test functions. We seek approximate solutions $u_0^h \in \mathcal{S}^h(\Omega)$ to the weak form, where $\mathcal{S}^h(\Omega)$ denotes a finite-dimensional approximation space.

Galerkin Approximations to Harmonic Shape Functions

Consider finite dimensional sub-spaces $\mathcal{S}^h(\Omega) \subset \mathcal{S}(\Omega)$ and $\mathcal{V}^h(\Omega) \subset \mathcal{V}(\Omega)$. The Galerkin approximation $u_0^h \in \mathcal{S}^h(\Omega)$ to a given harmonic shape function u_0 satisfies

$$\int_\Omega \nabla u_0^h \cdot \nabla v_0^h \, dV = \int_\Omega f v_0^h \, dV \quad \forall v_0^h \in \mathcal{V}^h(\Omega). \tag{3.9}$$

Bishop has already explored such an approximation scheme using an FE discretization of a given polyheral element into sub-dividing tetrahedra. Moreover, it was demonstrated in [4] that the resulting shape function approximations preserve low-order polynomial completeness.

Non-conforming Galerkin Approximations to Harmonic Shape Functions

If $\mathcal{S}^h(\Omega) \not\subset \mathcal{S}(\Omega)$ and $\mathcal{V}^h(\Omega) \not\subset \mathcal{V}(\Omega)$, in particular when $u_0^h \neq u_b$ and $v_0^h \neq 0$ on $\partial\Omega$, then we must resort to the use of non-conforming approximation methods.

One approach would be to consider a Lagrange multiplier method to weakly enforce the boundary condition $u_0 = u_b$ on $\partial\Omega$ via

$$\min_{u_0, \, \lambda} \mathcal{G}(u_0, \lambda), \tag{3.10}$$

$$\mathcal{G}(u_0, \lambda) \equiv \frac{1}{2} \int_\Omega \nabla u_0 \cdot \nabla u_0 \, dV - \int_\Omega f u_0 \, dV + \int_{\partial\Omega} [u_0 - u_b] \, \lambda \, dA, \tag{3.11}$$

yielding two sets of equations in terms of the approximation $u_0^h \in \mathcal{S}^h(\Omega)$ and the Lagrange multiplier field $\lambda \in \Lambda(\partial\Omega)$:

$$\int_\Omega \nabla u_0^h \cdot \nabla v_0^h \, dV - \int_\Omega f v_0^h \, dV + \int_{\partial\Omega} \lambda v_0^h \, dA = 0 \quad \forall v_0^h \in \mathcal{V}^h(\Omega), \tag{3.12}$$

$$\int_{\partial\Omega} (u_0^h - u_b) \, \delta\lambda \, dA = 0 \quad \forall \delta\lambda \in \Lambda(\partial\Omega). \tag{3.13}$$

Suppose that we establish bases for u_0^h and λ:

$$u_0^h = \sum_{a=1}^{N} \varphi_a u_a, \quad \lambda = \sum_{a=1}^{M} \phi_a \lambda_a, \tag{3.14}$$

such that

$$\sum_{a=1}^{N}\left[\int_{\Omega}\nabla\varphi_a\cdot\nabla\varphi_b\,dV\right]u_a+\sum_{c=1}^{M}\left[\int_{\partial\Omega}\varphi_b\,\phi_c\,dA\right]\lambda_c=0\quad\forall b, \tag{3.15}$$

$$\sum_{b=1}^{N}\left[\int_{\partial\Omega}\phi_c\,\varphi_b\,dA\right]u_b=\int_{\partial\Omega}\bar{u}\,\phi_c\,dA\quad\forall c. \tag{3.16}$$

If we suppose that the boundary conditions can be written in terms of yet another basis, i.e.

$$\bar{u}=\sum_{a=1}^{N}\psi_a\bar{u}_a, \tag{3.17}$$

then

$$\sum_{b=1}^{N}\left[\int_{\partial\Omega_e}\phi_c\,\varphi_b\,dA\right]u_b=\sum_{a=1}^{M}\left[\int_{\partial\Omega_e}\psi_a\,\phi_c\,dA\right]\bar{u}_a\quad\forall c. \tag{3.18}$$

Given an appropriate selection for the indicated bases, we must solve the saddle-point problem, in matrix format:

$$\begin{bmatrix}\mathbf{K}&\mathbf{C}\\ \mathbf{C}^T&\mathbf{0}\end{bmatrix}\begin{Bmatrix}\mathbf{u}\\ \boldsymbol{\lambda}\end{Bmatrix}=\begin{Bmatrix}\mathbf{0}\\ \mathbf{B}\bar{\mathbf{u}}\end{Bmatrix}, \tag{3.19}$$

where

$$K_{ab}=\int_{\Omega_e}\nabla_X\varphi_a\cdot\nabla_X\varphi_b\,dV,\quad C_{bc}=\int_{\partial\Omega_e}\varphi_b\,\phi_c\,dA,\quad B_{ac}=\int_{\partial\Omega_e}\psi_a\,\phi_c\,dA. \tag{3.20}$$

3.3 Break

Ultimately, one must show either that $\mathcal{S}^h$ and $\mathcal{V}^h$ and sub-spaces of $\mathcal{S}$ and $\mathcal{V}$, or else that any exterior approximation methods converge to the exact solution under cell refinement. Moreover, we must show that any approximation to the exact solution will yield elements that exhibit convergence under mesh (element) refinement – and interesting embedded convergence problem.

Harmonic shape functions φ satisfy the following partial differential equation on each polytopal element domain Ω_e:

$$\nabla_X^2\varphi=0\quad\forall\mathbf{X}\in\Omega_e, \tag{3.21}$$

subject to the Dirichlet boundary conditions:

$$\varphi=\bar{\varphi}\quad\forall\mathbf{X}\in\partial\Omega_e, \tag{3.22}$$

where it is supposed that the boundary conditions are informed by the values of the shape functions defined at the elements' nodes. Harmonic shape functions which satisfy the above are uniquely defined, and possess a number of desirable properties: smoothness, C^0 continuity at element boundaries, partition of unity, and polynomial reproducibility.

The notion that the shape functions define a set of smooth and continuous interpolants on an element is an appealing concept, though it can frequently lead to numerical complications (nearly-singular solutions), particularly if the elements possess degenerate geometric features. Herein we postulate a number of alternative boundary value problems for constructing shape functions on arbitrary polytopes. These formulations are informed by the conditions of *weak compatibility*, discussed in the following section.

An equivalent set of weakened boundary conditions may be written as

$$\int_{\partial\Omega_e} [u - \bar{u}]\, \lambda \, dA = 0 \quad \forall \lambda \in H^{1/2}(\partial\Omega_e), \tag{3.23}$$

where λ denotes a Lagrange multiplier field, and

$$H^{1/2}(\partial\Omega_e) \equiv \left\{ \lambda \in L^2(\partial\Omega_e) \,|\, \exists\, \lambda' \in H^1(\Omega_e) : \lambda = \mathrm{tr}(\lambda') \right\}. \tag{3.24}$$

A weak statement of the above equations can be written as

$$\int_{\Omega_e} \nabla_X u \cdot \nabla_X v \, dV = 0 \quad \forall v \in H_0^1(\Omega_e). \tag{3.25}$$

If we partition Ω_e into cells $\cup_i K_i$, we observe that

$$\int_{\Omega_e} \nabla_X u \cdot \nabla_X v \, dV = \sum_j \int_{\Gamma_j} v [\![\nabla_X u \cdot \mathbf{N}]\!] \, dA = 0 \quad \forall v \in H_0^1(\Omega_e). \tag{3.26}$$

If $[\![\nabla_X u \cdot \mathbf{N}]\!] = 0$, the above conditions are trivially satisfied. By contrast, to trivially satisfy compatibility in a weak sense, we insist that $[\![u]\!] = 0$ everywhere. We can consider enforcing both of these conditions in a weighted sense, resulting in the common PEM formulation in current usage:

$$\mathcal{F} = \sum_j \int_{\Gamma_j} \alpha_j [\![u]\!]^2 \, dA + \sum_j \int_{\Gamma_j} \beta_j [\![\nabla_X u \cdot \mathbf{N}]\!]^2 \, dA. \tag{3.27}$$

If $\alpha_j \gg \beta_j$, we obtain a field which satisfies compatibility preferrentially, whereas if $\alpha_j \ll \beta_j$, we satisfy Laplace's equation. The importance of compatibility is to guarantee

that the shape functions span a set of admissible solutions to the original BVP, whereas satisfaction of Laplace's equation guarantees uniqueness of the resulting shape functions.

Alternatively, if we pose an objective functional

$$\mathcal{F}(u,\lambda) = \frac{1}{2}\int_{\Omega_e} \nabla_X u \cdot \nabla_X u \, dV + \int_{\partial\Omega_e} [u - \bar{u}]\,\lambda \, dA, \tag{3.28}$$

it yields

$$\int_{\Omega_e} \nabla_X u \cdot \nabla_X \delta u \, dV + \int_{\partial\Omega_e} \delta u \, \lambda \, dA = 0 \quad \forall \delta u, \tag{3.29}$$

$$\int_{\partial\Omega_e} u \, \delta\lambda \, dA = \int_{\partial\Omega_e} \bar{u} \, \delta\lambda \, dA \quad \forall \delta\lambda. \tag{3.30}$$

Suppose that we establish bases for u and λ:

$$u = \sum_{a=1}^{N} \varphi_a u_a, \quad \lambda = \sum_{a=1}^{M} \phi_a \lambda_a, \tag{3.31}$$

such that

$$\sum_{a=1}^{N} \left[\int_{\Omega_e} \nabla_X \varphi_a \cdot \nabla_X \varphi_b \, dV \right] u_a + \sum_{c=1}^{M} \left[\int_{\partial\Omega_e} \varphi_b \, \phi_c \, dA \right] \lambda_c = 0 \quad \forall b, \tag{3.32}$$

$$\sum_{b=1}^{N} \left[\int_{\partial\Omega_e} \phi_c \, \varphi_b \, dA \right] u_b = \int_{\partial\Omega_e} \bar{u} \, \phi_c \, dA \quad \forall c. \tag{3.33}$$

If we suppose that the boundary conditions can be written in terms of yet another basis, i.e.

$$\bar{u} = \sum_{a=1}^{N} \psi_a \bar{u}_a, \tag{3.34}$$

then

$$\sum_{b=1}^{N} \left[\int_{\partial\Omega_e} \phi_c \, \varphi_b \, dA \right] u_b = \sum_{a=1}^{M} \left[\int_{\partial\Omega_e} \psi_a \, \phi_c \, dA \right] \bar{u}_a \quad \forall c. \tag{3.35}$$

Given an appropriate selection for the indicated bases, we must solve the saddle-point problem, in matrix format:

$$\begin{bmatrix} \mathbf{K} & \mathbf{C} \\ \mathbf{C}^T & \mathbf{0} \end{bmatrix} \begin{Bmatrix} \mathbf{u} \\ \boldsymbol{\lambda} \end{Bmatrix} = \begin{Bmatrix} \mathbf{0} \\ \mathbf{B}\bar{\mathbf{u}} \end{Bmatrix}, \tag{3.36}$$

where

$$K_{ab} = \int_{\Omega_e} \nabla_X \varphi_a \cdot \nabla_X \varphi_b \, dV, \quad C_{bc} = \int_{\partial\Omega_e} \varphi_b \, \phi_c \, dA, \quad B_{ac} = \int_{\partial\Omega_e} \psi_a \, \phi_c \, dA. \tag{3.37}$$

The generalized patch test requires that

$$\lim_{h\to 0}\sum_e \int_{\Omega_e} \psi\, u\, \mathbf{n}\, dA = 0 \quad \forall \psi \in C_0^\infty. \tag{3.38}$$

Let us momentarily consider the case when each element is bounded by some $d-1$ dimensional manifold, upon which we presume that the shape functions are well-defined as $\bar{u}$. Upon any given element domain, we insist that

$$\lim_{h\to 0}\int_{\Omega_e} \psi\, [\![u]\!]\, \mathbf{n}\, dA = 0 \quad \forall \psi \in C^\infty \tag{3.39}$$

must hold for the generalized patch test to be satisfied, where $[\![u]\!] = u - \bar{u}$. Suppose we define projection operators $\Pi : C^\infty(\Omega_e) \to P^k(\Omega_e)$ and $\pi : C^\infty(\Omega_e) \to C^\infty(\Omega_e)\backslash P^k(\Omega_e)$ such that

$$u = \Pi u + \pi u, \quad \psi = \Pi\psi + \pi\psi, \tag{3.40}$$

then

$$\int_{\Omega_e} \psi\, [\![u]\!]\, \mathbf{n}\, dA = \int_{\Omega_e} \Pi\psi\, \Pi[\![u]\!]\, \mathbf{n}\, dA + \int_{\Omega_e} \Pi\psi\, \pi[\![u]\!]\, \mathbf{n}\, dA \tag{3.41}$$

$$+ \int_{\Omega_e} \pi\psi\, \Pi[\![u]\!]\, \mathbf{n}\, dA + \int_{\Omega_e} \pi\psi\, \pi[\![u]\!]\, \mathbf{n}\, dA. \tag{3.42}$$

It can be shown that

$$\int_{\Omega_e} \Pi\psi\, \Pi[\![u]\!]\, \mathbf{n}\, dA = 0 \quad \forall \psi \in C^\infty \tag{3.43}$$

if the function defined on the element's boundary is sufficiently smooth, and can represent polynomial fields up to order k. Consequently,

$$\int_{\Omega_e} \psi\, [\![u]\!]\, \mathbf{n}\, dA = \int_{\Omega_e} \Pi\psi\, \pi[\![u]\!]\, \mathbf{n}\, dA \tag{3.44}$$

$$+ \int_{\Omega_e} \pi\psi\, \Pi[\![u]\!]\, \mathbf{n}\, dA + \int_{\Omega_e} \pi\psi\, \pi[\![u]\!]\, \mathbf{n}\, dA. \tag{3.45}$$

We effectively need to demonstrate passage of the E-1 and M-1 tests for convergence of nonconforming methods. Will need estimates for boundary integrals, or can demonstrate this numerically (preferred).

Weak Compatibility

Consider the necessary and sufficient conditions for compatibility of a deformation gradient field $\mathbf{F}$ stated in equation (2.6), reiterated:

$$\nabla_X \times \mathbf{F} = \mathbf{0} \quad \forall \mathbf{X} \in \mathcal{B}_0. \tag{3.46}$$

If the deformation gradient is computed from a set of basis functions $\{\varphi_a\}_{a=1}^N$ for the displacement field via

$$\mathbf{F} = \sum_{a=1}^{N} \mathbf{x}_a \otimes \nabla_X \varphi_a, \tag{3.47}$$

we arrive at a set of equivalent conditions on the basis functions:

$$\nabla_X \times \nabla_X \varphi = \mathbf{0} \quad \forall \mathbf{X} \in \mathcal{B}_0,\, \varphi \in \{\varphi_a\}_{a=1}^N. \tag{3.48}$$

These equations are trivially satisfied when the basis functions are $C^2(\mathcal{B}_0)$ continuous, and may therefore be used to construct admissible trial solutions to the strong form statement of equilibrium described in section 2.4.

In general, the construction of basis functions $\varphi \in C^2(\mathcal{B}_0)$ is not trivial. Moreover, we seek solutions to the weak form such that $\mathbf{u} \in H^1(\Omega)$. In what follows, we shall consider the space of functions $\varphi \in C^0(\mathcal{B}_0)$ satisfying a weakened statement of compatibility:

$$\int_{\mathcal{B}_0} (\nabla_X \times \nabla_X \varphi) \cdot \mathbf{v}\, dV = 0 \quad \forall \mathbf{v} \in C_0^\infty(\mathcal{B}_0). \tag{3.49}$$

Through repeated application of integration by parts, the condition that the test functions satisfy compatibility ($\nabla_X \times \nabla_X \mathbf{v} = \mathbf{0}\, \forall \mathbf{v} \in C_0^\infty(\mathcal{B}_0)$), and the divergence theorem, we determine

$$\int_{\mathcal{B}_0} \nabla_X \cdot (\nabla_X \varphi \times \mathbf{v})\, dV + \int_{\mathcal{B}_0} \nabla_X \varphi \cdot (\nabla_X \times \mathbf{v})\, dV = 0, \tag{3.50}$$

$$\int_{\mathcal{B}_0} \nabla_X \cdot (\nabla_X \times (\varphi \mathbf{v}))\, dV = \int_{\partial \mathcal{B}_0} (\nabla_X \times (\varphi \mathbf{v})) \cdot d\mathbf{A} = 0. \tag{3.51}$$

If we consider a partition $\mathcal{T}^h = \{\Omega_e\}_{e=1}^{N_e}$ of $\mathcal{B}_0$ into polytopal elements $\Omega_e \subset \mathcal{B}_0$ whose shape functions are assumed to be piece-wise smooth and continuous on element interiors, then we may impose the equivalent condition:

$$\sum_{e=1}^{N_e} \int_{\partial \Omega_e} (\nabla_X \times (\varphi|_{\Omega_e} \mathbf{v})) \cdot d\mathbf{A} = 0 \quad \forall \varphi,\, \mathbf{v} \in C_0^\infty(\mathcal{B}_0). \tag{3.52}$$

It it evident that if $[\![\varphi]\!] = \varphi|_{\Omega_a} - \varphi|_{\Omega_b} = 0 \, \forall \partial\Omega_a \cap \partial\Omega_b \neq \emptyset$, then the above condition is trivially satisfied. Such is the case for $C^0(\mathcal{B}_0)$ conforming finite element methods.

If $\varphi \not\subset C^0(\mathcal{B}_0)$, we require

$$\lim_{h\to 0} \sum_{e=1}^{N_e} \int_{\partial\Omega_e} (\nabla_X \times (\varphi|_{\Omega_e} \mathbf{v})) \cdot d\mathbf{A} = 0 \quad \forall \varphi, \, \mathbf{v} \in C_0^\infty(\mathcal{B}_0), \tag{3.53}$$

which is equivalent to

$$\lim_{h\to 0} \sum_{e=1}^{N_e} \int_{\partial\Omega_e} (\varphi|_{\Omega_e} (\nabla_X \times \mathbf{v}) + \nabla_X \varphi|_{\Omega_e} \times \mathbf{v}) \cdot d\mathbf{A} = 0 \quad \forall \varphi, \, \mathbf{v} \in C_0^\infty(\mathcal{B}_0). \tag{3.54}$$

Equivalently, we may enforce this condition over each individual face $\Gamma = \Omega_a \cap \Omega_b \neq \emptyset$, such that

$$\lim_{h\to 0} \int_{\Gamma} ([\![\varphi]\!] (\nabla_X \times \mathbf{v}) + \nabla_X [\![\varphi]\!] \times \mathbf{v}) \cdot d\mathbf{A} = 0 \quad \forall \Gamma, \, \mathbf{v} \in C_0^\infty(\mathcal{B}_0). \tag{3.55}$$

We may expand $[\![\varphi]\!] = a_0 + \mathbf{a}_1 \cdot \mathbf{X} + O(\mathbf{X}^2)$ and $\mathbf{v} = \mathbf{b}_0 + \mathbf{B}_1 \mathbf{X} + O(\mathbf{X}^2)$ in terms of low-order polynomials to illustrate

$$\lim_{h\to 0} \int_{\Gamma} ((a_0 + \mathbf{a}_1 \cdot \mathbf{X}) \mathbf{B}_1 + \mathbf{a}_1 \times (\mathbf{b}_0 + \mathbf{B}_1 \mathbf{X})) \cdot d\mathbf{A} = 0 \quad \forall \Gamma, \, \mathbf{v} \in C_0^\infty(\mathcal{B}_0). \tag{3.56}$$

$$\lim_{h\to 0} \sum_{e=1}^{N_e} \int_{\partial\Omega_e} (\varphi|_{\Omega_e} (\nabla_X \times \mathbf{v})) \cdot d\mathbf{A} - \sum_{e=1}^{N_e} \int_{\Omega_e} \nabla_X \varphi|_{\Omega_e} \cdot (\nabla_X \times \mathbf{v}) \, dV = 0 \quad \forall \varphi, \, \mathbf{v} \in C_0^\infty(\mathcal{B}_0), \tag{3.57}$$

and because $\nabla_X \times : C_0^\infty(\mathcal{B}_0) \mapsto C_0^\infty(\mathcal{B}_0)$, we have

$$\lim_{h\to 0} \sum_{e=1}^{N_e} \int_{\partial\Omega_e} \varphi|_{\Omega_e} \mathbf{v} \cdot d\mathbf{A} - \sum_{e=1}^{N_e} \int_{\Omega_e} \mathbf{v} \cdot \nabla_X \varphi|_{\Omega_e} \, dV = 0 \quad \forall \varphi, \, \mathbf{v} \in C_0^\infty(\mathcal{B}_0). \tag{3.58}$$

Recognizing that

$$\int_{\Omega_e} \mathbf{v} \cdot \nabla_X \varphi|_{\Omega_e} \, dV \leq ||\nabla_X \varphi|_{\Omega_e}||^2_{\Omega_e}, \tag{3.59}$$

If we insist on

$$\sum_{e=1}^{N_e} \int_{\partial\Omega_e} (\nabla_X \times (\varphi|_{\Omega_e} \mathbf{v})) \cdot d\mathbf{A} = 0 \quad \forall \varphi, \, \mathbf{v} \in P^1(\mathcal{B}_0), \tag{3.60}$$

i.e. if we expand $\mathbf{v} = \mathbf{v}_0 + \mathbf{V}_1 \mathbf{x}$ and

$$\sum_{e=1}^{N_e} \int_{\partial\Omega_e} (\nabla_X \times (\varphi|_{\Omega_e} \mathbf{v})) \cdot d\mathbf{A} = 0 \quad \forall \varphi, \, \mathbf{v} \in P^1(\mathcal{B}_0), \tag{3.61}$$

3.4 The Partitioned Element Framework

The Element Partition

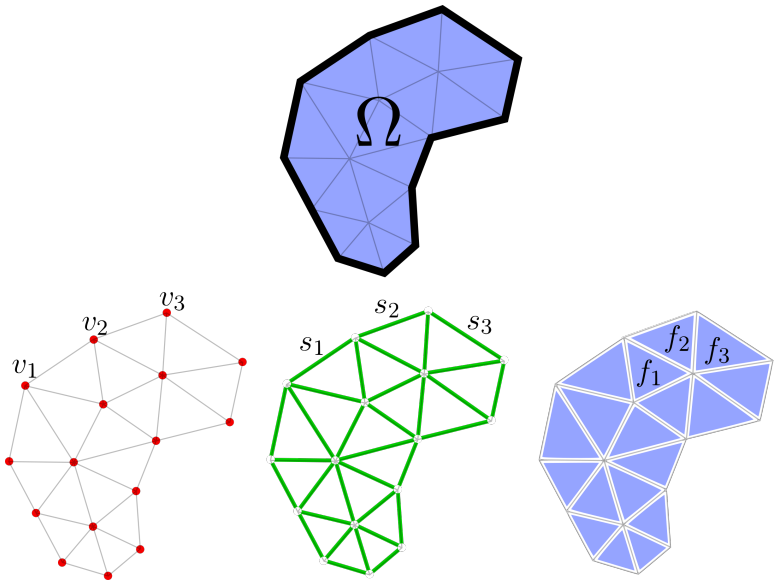

Figure 3.1. A representative domain $\Omega \subset \mathbb{R}^2$, and it's corresponding partition into verticies, segments, and facets.

- Provide a figure of an element with partitioned geometry
- Define partitioned geometry terms (cells, facets, segments, verticies, etc.), perhaps even give a table of definitions, all referring back to the main figure(s)
-

3.4.1 Partition-Based Approximation Spaces

FE basis

WG basis

DG basis

VE basis

Traditional approximation methods typically consider the independent specification of two principal transformations: an interpolation scheme, which is necessary to represent field variables according to known point-values; and a quadrature rule, for the purposes of integrating such fields over the domain on which they are defined.

In mathematical terms, an interpolant φ is a linear operator which maps vectors $\mathbf{u} \in \mathbb{R}^k$ containing point-wise data regarding a field into scalar functions $f \in V^k(\Omega)$, i.e.

$$\varphi \colon \mathbb{R}^k \mapsto V^k(\Omega) \tag{3.62}$$

where $\mathbb{R}^k$ is a k-dimensional real space, and $V^k(\Omega)$ is a k-dimensional function space defined on Ω.

By constrast, a quadrature rule Σ is a linear operator which maps scalar functions $f \in V^k(\Omega)$ to vectors $\mathbf{q} \in \mathbb{R}^p$ identifying point-wise samples of f, i.e.

$$\Sigma \colon V^k(\Omega) \mapsto \mathbb{R}^p \tag{3.63}$$

The composition $\Sigma \circ \varphi$ of an interpolant φ with a quadrature rule Σ yields a linear operator

$$\Sigma \circ \varphi \colon \mathbb{R}^k \mapsto \mathbb{R}^p \tag{3.64}$$

3.4.2 Partition-Based Quadrature Rules

If arbitrary polytopal shapes are to be used as elements in the PEM, then we must devise a means of integrating contributions to the weak form , ostensibly through the use of quadrature rules on the elements' interiors and boundaries. Such rules must be sufficiently stable (utilizing a sufficient number of well-positioned quadrature points) and accurate (capable of exactly integrating low-order polynomials up to some specified degree).

Partitioned element methods proceed by partitioning the elements (and their boundaries) into a sufficient number of polytopal sub-domains which are used as integration cells. Low-order (i.e. 1-point) quadrature rules are defined on each of these sub-domains, and a composite quadrature rule for the element is assembled from the collection of all quadrature points in each sub-domain. In general, these quadrature rules will need to be modified to satisfy Galerkin exactness for certain low-order polynomial solutions.

Methods for partitioning the elements into sub-domains which yield stable and efficient composite quadrature rules are discussed in the following section. Later discussion is given to the correction of these quadratures for the sake of satisfying Galerkin exactness (quadrature consistency).

Composite Quadrature Rules

Given a partition of the elements into sub-domains (quadrature cells), one may utilize a low order quadrature rule over each sub-domain, thereby yielding a composite quadrature rule over the element as a whole, whose overall accuracy is determined by the order of accuracy used in each sub-domain.

The simplest quadrature rule of this form is a composite mid-point scheme, where the quadrature points are located at the centroids of each sub-domain. Such a rule exactly integrates polynomials up to first order, and is otherwise reasonably accurate. The integration points are guaranteed to be interior to each sub-domain (and the element as a whole) provided each cell is convex.

For simple sub-divisions (consisting of triangles or tetrahedra), composite quadrature rules may be extended to obtain high-order accuracy. For generic sub-divisions (consiting of arbitrary polytopes), the extension to high-order is not clear. For this reason, we will focus attention on composite mid-point rules.

A number of different partitioning schemes are illustrated in Figure 3.2. In general,

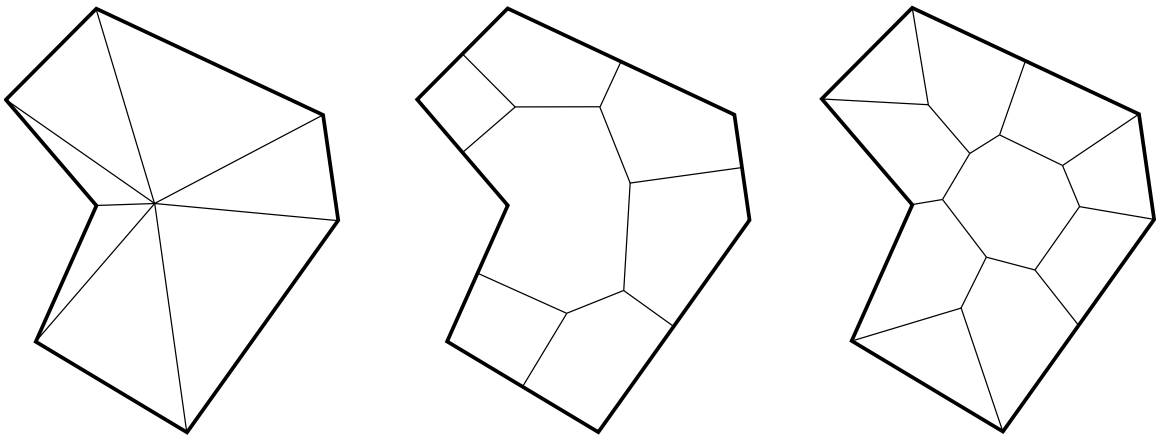

Figure 3.2. Various element partitioning schemes. From left to right: edge-based partition, node-based partition, voronoi partition.

the resulting cells ω may possess arbitrary polytopal shape, whose centroids $\bar{\mathbf{X}}$ may be computed via

$$\bar{\mathbf{X}} = \frac{\int_\omega \mathbf{X}\, dV}{\int_\omega dV}. \tag{3.65}$$

We may compute polynomial moments on any arbitrary polytope using the method pro-

posed by Lasserre et al. in [9], such that

$$\int_{\omega} \mathbf{X}^{\alpha}\, dV = \frac{1}{d+|\alpha|} \int_{\partial\omega} (\mathbf{X}\cdot\mathbf{N})\, \mathbf{X}^{\alpha}\, dA. \tag{3.66}$$

Selective Modal Quadrature

Consider all functions $f \in L^2(\Omega)$ represented over an arbitrary polytopal element domain $\Omega \subset \mathbb{R}^d$. Standard quadrature rules approximate the integral of f over Ω as

$$\int_{\Omega} f\, dv \approx \sum_{q=1}^{N_{qp}} w_q f(\mathbf{x}_q). \tag{3.67}$$

Consider an $L^2(\Omega)$ polynomial projection operator $\Pi : L^2 \mapsto P^k$ which may be used to decompose $f = f_p + f_n$ into polynomial and non-polynomial parts:

$$f_p = \Pi f, \quad f_n = f - \Pi f = \pi f, \tag{3.68}$$

where $\pi : L^2 \mapsto L^2 \backslash P^k$. Consequently, we observe that Πf is L^2 orthogonal to any πg for all $g \in L^2$, to the extent that

$$\int_{\Omega} (\Pi f)(g - \Pi g)\, dv = \langle \Pi f, g - \Pi g \rangle_{\Omega} = 0 \quad \forall f,\, g \in L^2. \tag{3.69}$$

We propose a quadrature rule of the form:

$$\int_{\Omega} f\, dv \approx \int_{\Omega} f_p\, dv + \sum_{q=1}^{N_{qp}} w_q f_n(\mathbf{x}_q), \tag{3.70}$$

where it is supposed that $\int_{\Omega} f_p\, dv$ may be computed exactly using the methodology proposed by Lasserre in [9]. Further, if we wish to integrate the product fg where $f,\, g \in H^1(\Omega)$, we may write

$$\int_{\Omega} fg\, dv = \langle f, g \rangle_{\Omega} = \langle \Pi f + \pi f, \Pi g + \pi g \rangle_{\Omega}, \tag{3.71}$$

which, by the linearity of the L_2 inner product, and by the orthogonality of Πf and πg (and of πf and Πg), yields

$$\int_{\Omega} fg\, dv = \langle \Pi f, \Pi g \rangle_{\Omega} + \langle \pi f, \pi g \rangle_{\Omega}, \tag{3.72}$$

and thus

$$\int_\Omega f g \, dv \approx \int_\Omega f_p g_p \, dv + \sum_{q=1}^{N_{qp}} w_q f_n(\mathbf{x}_q) g_n(\mathbf{x}_q). \tag{3.73}$$

This is effectively equivalent to integrating the product of all low-order polynomials exactly, while integrating the product of all non-polynomial "remainders" only approximately, using a quadrature rule.

If we are only given point evaluations of a function f at $\{\mathbf{x}_q\}_{q=1}^{N_{qp}}$, then we must construct a low-order polynomial projection operator by considering the least-squares problem:

$$\min_{f_p \in P^k(\Omega)} \frac{1}{2} ||f_p - f||_\Omega^2, \tag{3.74}$$

where $||f||_\Omega = \sqrt{\langle f, f \rangle_\Omega}$ is deliberately approximated using the element's quadrature rule:

$$\langle f, f \rangle_\Omega \approx \sum_{q=1}^{N_{qp}} w_q \left[f(\mathbf{x}_q) \right]^2. \tag{3.75}$$

For a given polynomial basis $\{z_a\}_{a=1}^{K}$ which spans $P^k(\Omega)$, we may write

$$f_p(\mathbf{x}) = \sum_{a=1}^{K} z_a(\mathbf{x}) c_a = \mathbf{z}^T(\mathbf{x}) \, \mathbf{c}, \tag{3.76}$$

and the solution to (3.75) satisfies

$$\sum_{a=1}^{K} \sum_{q=1}^{N_{qp}} w_q z_b(\mathbf{x}_q) z_a(\mathbf{x}_q) c_a = \sum_{q=1}^{N_{qp}} w_q z_b(\mathbf{x}_q) f(\mathbf{x}_q) \quad \forall b = 1, \ldots, K, \tag{3.77}$$

which may be written in matrix form as $\mathbf{Z}^T \mathbf{W} \mathbf{Z} \mathbf{c} = \mathbf{Z}^T \mathbf{W} \mathbf{f}$, where we denote $f_i = f(\mathbf{x}_i)$, $W_{ii} = w_i$, $W_{ij} = 0 \, \forall i \neq j$, and $Z_{ij} = z_j(\mathbf{x}_i)$. The discrete polynomial projection operator $\mathbf{\Pi} : \mathbb{R}^{N_{qp}} \mapsto \mathbb{R}^K$ is computed as $\mathbf{\Pi} = (\mathbf{Z}^T \mathbf{W} \mathbf{Z})^{-1} \mathbf{Z}^T \mathbf{W}$, and the complement operator $\boldsymbol{\pi} : \mathbb{R}^{N_{qp}} \mapsto \mathbb{R}^{N_{qp}}$ is $\boldsymbol{\pi} = \mathbf{1}_{N_{qp}} - \mathbf{\Pi}^\dagger \mathbf{\Pi}$. Consequently,

$$\langle \Pi f, \Pi g \rangle_\Omega = \langle \mathbf{z}^T \mathbf{\Pi} \mathbf{f}, \mathbf{z}^T \mathbf{\Pi} \mathbf{g} \rangle_\Omega = \mathbf{f}^T \left[\mathbf{\Pi}^T \left(\int_\Omega \mathbf{z} \otimes \mathbf{z} \, dv \right) \mathbf{\Pi} \right] \mathbf{g} = \mathbf{f}^T \mathbf{W}_p \mathbf{g}, \tag{3.78}$$

$$\langle \pi f, \pi g \rangle_\Omega \approx \sum_{q=1}^{N_{qp}} w_q f_n(\mathbf{x}_q) g_n(\mathbf{x}_q) = \mathbf{f}^T \left[\boldsymbol{\pi}^T \mathbf{W} \boldsymbol{\pi} \right] \mathbf{g} = \mathbf{f}^T \mathbf{W}_n \mathbf{g}, \tag{3.79}$$

$$\int_\Omega f g \, dv \approx \mathbf{f}^T(\mathbf{W}_p + \mathbf{W}_n)\mathbf{g} = \mathbf{f}^T\mathbf{M}\mathbf{g} = \sum_{q=1}^{N_{qp}} \sum_{p=1}^{N_{qp}} M(\mathbf{x}_q, \mathbf{x}_p)\, f(\mathbf{x}_q)\, g(\mathbf{x}_p). \tag{3.80}$$

We shall refer to this form of integration as *selective modal quadrature*, in that particular low-order polynomial modes are integrated exactly, and any higher modes are approximated using the element's quadrature rules. The advantage of modal quadrature is that we may exactly integrate any terms which directly impact quadrature consistency, and hence, virtually any stable quadrature may be used to integrate the higher-order part.

Rather than storing the independent quadrature weights $w_q = w(\mathbf{x}_q)$, selective modal quadrature requires the storage of a generalized quadrature weighting matrix $M(\mathbf{x}_q, \mathbf{x}_p)$. Alternatively, for the sake of efficiency, if the function g is known a priori (e.g. if g is a test function for a weighted residual method), then we need only store the "augmented" test function values:

$$\tilde{g}(\mathbf{x}_q) = \sum_{p=1}^{N_{qp}} \frac{M(\mathbf{x}_q, \mathbf{x}_p)}{w_q}\, g(\mathbf{x}_p), \tag{3.81}$$

and all integrals involving f and g may be carried out via

$$\int_\Omega f g \, dv \approx \sum_{q=1}^{N_{qp}} w_q\, \tilde{g}(\mathbf{x}_q)\, f(\mathbf{x}_q), \tag{3.82}$$

which is effectively equivalent to a gradient correction scheme, similar to the method proposed in [47].

3.4.3 Selection of an Appropriate Objective Functional

Once we have specified a given approximation space of functions, our goal is then to select the function from this space which best represents the nodal data that we are attempting to interpolate over the element. The essential question is this: by what metric should we objectively assess the appropriateness of a given approximating function?

Construction of Element Appoximants

3.5 Essential Requirements of the PEM

Reproducibility

Fundamentally, the approximation power of the PEM depends directly upon the degree of completeness of the underlying approximation space. In particular, the finite-dimensional

trial solution space $\mathcal{S}^h$ should contain as a subspace $\mathbb{P}_k \subset \mathcal{S}^h$ for some $k \geq 0$, where $\mathbb{P}_k$ denotes the subspace of polynomial functions with maximal degree k. This guarantees that the PEM approximation space will be capable of exactly reproducing any polynomial function up to some specified order.

Requirements of the Approximation Space

Compatibility

Weak Compatibility

Stability

Restrictions on the Element Partition

Variational Consistency

Weak Enforcement of Consistency

Recall the α-th order variational consistency requirements:

$$\int_\Omega \mathbf{x}^\alpha \varphi_{a,i}\, dv + \int_\Omega \mathbf{x}^\alpha_{,i} \varphi_a\, dv = \int_{\partial\Omega} \mathbf{x}^\alpha n_i \varphi_a\, da \quad \forall i, a. \tag{3.83}$$

This degree of consistency is required for all $|\alpha| \leq k-1$ if the bi-linear form $a : \mathcal{S}\times\mathcal{V} \mapsto \mathbb{R}$ is to determine uniqueness of any exact polynomial solutions up to order k contained within $\mathcal{S}^h \supset P_k$. Moreover, the above expression implies that any solution may be reasonably well approximated by low-order polynomials in the locality of the selected domain Ω.

Consequently, we may consider an application of the above consistency requirements to the entire problem domain Ω, or – more practically – we may enforce consistency up to the desired order on each element domain Ω_e. The element-local α-th order consistency equations follow:

$$\int_{\Omega_e} \mathbf{x}^\alpha \varphi_{a,i}\, dv + \int_{\Omega_e} \mathbf{x}^\alpha_{,i} \varphi_a\, dv = \int_{\partial\Omega_e} \mathbf{x}^\alpha n_i \varphi_a\, da \quad \forall i, a. \tag{3.84}$$

In most practical situations, it may not be possible to evaluate the integral expressions exactly. Instead, numerical quadrature rules must be defined, both on the element's interior, and on its boundary, such that

$$\int_{\Omega_e} f(\mathbf{x}) dv \approx \sum_{q=1}^{N_q} w_q f(\mathbf{x}_q), \quad \int_{\partial\Omega_e} f(\mathbf{x}) da \approx \sum_{b=1}^{N_b} w_b f(\mathbf{x}_b). \tag{3.85}$$

This yields yet another form of consistency, henceforth referred to as "quadrature consistency," expressed as:

$$\sum_{q=1}^{N_q} w_q \left[\mathbf{x}_q^\alpha \varphi_{a,i}^{(q)} + \mathbf{x}_{q,i}^\alpha \varphi_a^{(q)} \right] = \sum_{b=1}^{N_b} w_b \mathbf{x}_b^\alpha n_i^{(b)} \varphi_a^{(b)} \quad \forall i, a. \tag{3.86}$$

Moving forward in our developments, quadrature consistency will be the only form of consistency of practical interest, as it appropriately reflects the discrete data quantities at our disposal.

A brief remark should be made regarding the lack of equivalence between the exact evaluation of consistency in equation (3.84) and its numerical approximation in equation (3.86). In general, we cannot claim that satisfaction of one guarantees the other. There is only one occasion when we may say that (3.86) holds if and only if (3.84) is satisfied, which occurs only when sufficiently accurate quadrature rules are used on the element and its boundary. In the vast majority of situations, however, this is an impractical constraint, as the construction of high-order quadrature rules on arbitrary polyhedra (though possible) proves to be somewhat computationally intensive (see the literature by Sukumar, etc.). Moreover, without a precise representation of the test functions over the element domain, it becomes infeasible to consider an exact integration of such functions.

Numerical Quadrature Consistency

Beyond consistency with the weak form for a specified subspace of polynomial functions used to represent the solution, we also require that the numerical quadrature scheme utilized be sufficiently accurate to the extent that: Galerkin exactness is satisfied for certain classes of solutions, and that the quadrature error has a bound which is of a lower order than that of the approximation error.

Chapter 4

An Implementational Framework for the PEM

Chapter 5

A Numerical Evaluation of the PEM

5.1 Convergence Analysis

5.2 Parameter Sensitivity Analysis

5.3 Computational Efficiency

5.3.1 Performance Comparison

5.4 Resistance to Locking Phenomena

Chapter 6

Conclusions and Future Work

Evaluate the efficacy of the proposed formulations within the presented context. Assess whether there really is a silver bullet to the locking problem, or if we can expect for locking to be an inherrent issue with any numerical approximation method.

Describe the nature of future work that will be done in this area of research.

References

[1] Ivo Babuška. Error-bounds for finite element method. *Numerische Mathematik*, 16:322–333, 1971.

[2] Ivo Babuška and Manil Suri. Locking effects in the finite element approximation of elasticity problems. *Numerische Mathematik*, 62:439–463, 1992.

[3] Ivo Babuška and Manil Suri. On locking and robustness in the finite element method. *SIAM Journal on Numerical Analysis*, 29(5):1261–1293, 1992.

[4] J. E. Bishop. A displacement-based finite element formulation for general polyhedra using harmonic shape functions. *International Journal for Numerical Methods in Engineering*, 97:1–31, 2014.

[5] Franco Brezzi. On the existence, uniqueness and approximation of saddle-point problems arising from lagrangian multipliers. *ESAIM: Mathematical Modelling and Numerical Analysis - Modlisation Mathmatique et Analyse Numrique*, 8:129–151, 1974.

[6] Jiun-Shyan Chen, Michael Hillman, and Marcus Rüter. An arbitrary order variationally consistent integration for galerkin meshfree methods. *International Journal for Numerical Methods in Engineering*, 95:387–418, 2013.

[7] H. Chi, L. Beirão da Veiga, and G. H. Paulino. Some basic formulations of the virtual element method (vem) for finite deformations. *Computer Methods in Applied Mechanics and Engineering*, 318:148–192, 2017.

[8] Heng Chi, Cameron Talischi, Oscar Lopez-Pamies, and Glaucio H. Paulino. A paradigm for higher-order polygonal elements in finite elasticity using a gradient correction scheme. *Computer Methods in Applied Mechanics and Engineering*, 306:216–251, 2016.

[9] Eric B. Chin, Jean B. Lasserre, and N. Sukumar. Numerical integration of homogeneous functions on convex and nonconvex polygons and polyhedra. *Computational Mechanics*, 56:967–981, 2015.

[10] Zhong ci Shi. The f-e-m-test for convergence of nonconforming finite elements. *Mathematics of Computation*, 49(180):391–405, 1987.

[11] L. Beirão da Veiga, F. Brezzi, A. Cangiani, G. Manzini, L. D. Marini, and A. Russo. Basic principles of virtual element methods. *Computer Methods in Applied Mechanics and Engineering*, 23:199–214, 2013.

[12] L. Beirão da Veiga, C. Lovadina, and D. Mora. A virtual element method for elastic and inelastic problems on polytope meshes. *Computer Methods in Applied Mechanics and Engineering*, 295:327–346, 2015.

[13] E. A. de Souza Neto, D. Perić, M. Dukto, and D. R. J. Owen. Design of simple low order finite elements for large strain analysis of nearly incompressible solids. *International Journal of Solids and Structures*, 33:3277–3296, 1996.

[14] C. R. Dohrmann and M. M. Rashid. Polynomial approximation of shape function gradients from element geometries. *International Journal for Numerical Methods in Engineering*, 53:945–958, 2002.

[15] Mohamed Salah Ebeida. Vorocrust v. 1.0, Jul 2017.

[16] Carlos A. Felippa. *Introduction to Finite Element Methods*. University of Colorado, Boulder, 2004.

[17] D. P. Flanagan and T. Belytschko. A uniform strain hexahedron and quadrilateral with orthogonal hourglass control. *International Journal for Numerical Methods in Engineering*, 17:679–706, 1981.

[18] Michael S. Floater. Mean value coordinates. *Computer Aided Geometric Design*, 20:19–27, 2003.

[19] Arun Gain, Cameron Talischi, and Glaucio H. Paulino. On the virtual element method for three-dimensional elasticity problems on arbitrary polyhedral meshes. *Computer Methods in Applied Mechanics and Engineering*, 282, 11 2013.

[20] Xifeng Gao, Wenzel Jakob, Marco Tarini, and Daniele Panozzo. Robust hex-dominant mesh generation using field-guided polyhedral agglomeration. *ACM Transactions on Graphics*, 36, 2017.

[21] William J. Gordon and James A. Wixom. Pseudo-harmonic interpolation on convex domains. *SIAM Journal on Numerical Analysis*, 11(5):909–933, 1974.

[22] Thomas J. R. Hughes. *The Finite Element Method–Linear Static and Dynamic Finite Element Analysis*. Dover Publications, 2000.

[23] Pushkar Joshi, Mark Meyer, Tony DeRose, Brian Green, and Tom Sanocki. Harmonic coordinates for character articulation. *ACM Transactions on Graphics*, 26, 2007.

[24] Nam-Sua Lee and Klaus-Jürgen Bathe. Effects of element distortions on the performance of isoparametric elements. *International Journal for Numerical Methods in Engineering*, 36:3553–3576, 1993.

[25] Qiaoluan H. Li and Junping Wang. Weak galerkin finite element methods for parabolic equations. *Numerical Methods for Partial Differential Equations*, 29:2004–2024, 2013.

[26] Guang Lin, Jiangguo Liu, and Farrah Sadre-Marandi. A comparative study on the weak galerkin, discontinuous galerkin, and mixed finite element methods. *Journal of Computational and Applied Mathematics*, 273:346–362, 2015.

[27] Richard H. MacNeal. A theorem regarding the locking of tapered four-noded membrane elements. *International Journal for Numerical Methods in Engineering*, 24:1793–1799, 1987.

[28] Sebastian Martin, Peter Kaufmann, Mario Botsch, Martin Wicke, and Markus Gross. Polyhedral finite elements using harmonic basis functions. *Eurographics Symposium on Geometry Processing 2008*, 27(5), 2008.

[29] L. Mu, J. Wang, and Y. Wang. A computational study of the weak galerkin method for second-order elliptic equations. *Numerical Algorithms*, 63:753, 2013.

[30] L. Mu, J. Wang, and X. Ye. Weak galerkin finite element method for second-order elliptic problems on polytopal meshes. *International Journal of Numerical Analysis and Modeling*, 12:31–53, 2015.

[31] Lin Mu, Junping Wang, and Xiu Ye. A weak galerkin finite element method with polynomial reduction. *Journal of Computational and Applied Mathematics*, 285:45–58, 2015.

[32] Daniel Pantuso and Klaus-Jürgen Bathe. On the stability of mixed finite elements in large strain analysis of incompressible solids. *Finite Elements in Analysis and Design*, 28:83–104, 1997.

[33] M. M. Rashid. Incremental kinematics for finite element applications. *International Journal for Numerical Methods in Engineering*, 36:3937–3956, 1993.

[34] M. M. Rashid and P. M. Gullett. On a finite element method with variable element topology. *Computer Methods in Applied Mechanics and Engineering*, 190:1509–1527, 2000.

[35] M. M. Rashid and A. Sadri. The partitioned element method in computational solid mechanics. *Computer Methods in Applied Mechanics and Engineering*, 237–240:152–165, 2012.

[36] M. M. Rashid and M. Selimotić. A three-dimensional finite element method with arbitrary polyhedral elements. *International Journal for Numerical Methods in Engineering*, 67:226–252, 2006.

[37] J.-F. Remacle, J. Lambrechts, B. Seny, E. Marchandise, A. Johnen, and C. Geuzainet. Blossom-quad: a non-uniform quadrilateral mesh generator using a minimum cost perfect matching algorithm. *International Journal for Numerical Methods in Engineering*, 89:1102–1119, 2012.

[38] Mili Selimotić. *Polyhedral Finite-Element Approximants in 3D Solid Mechanics*. PhD thesis, University of California, Davis, 2008.

[39] J. C. Simo and F. Armero. Geometrically non-linear enhanced strain mixed methods and the method of incompatible modes. *International Journal for Numerical Methods in Engineering*, 33:1413–1449, 1992.

[40] J. C. Simo, F. Armero, and R. L. Taylor. Improved versions of assumed enhanced strain tri-linear elements for 3d finite deformation problems. *Computer Methods in Applied Mechanics and Engineering*, 110:359–386, 1993.

[41] J. C. Simo and M. S. Rifai. A class of mixed assumed strain methods and the method of incompatible modes. *International Journal for Numerical Methods in Engineering*, 29:1595–1638, 1990.

[42] Friedrich Stummel. The generalized patch test. *SIAM Journal on Numerical Analysis*, 16(3):449–471, 1979.

[43] N. Sukumar. Construction of polygonal interpolants: a maximum entropy approach. *International Journal for Numerical Methods in Engineering*, 61:2159–2181, 2004.

[44] Manil Suri. On the robustness of the h- and p-versions of the finite-element method. *Journal of Computational and Applied Mathematics*, 35:303–310, 1991.

[45] Theodore Sussman and Klaus-Jürgen Bathe. Spurious modes in geometrically nonlinear small displacement finite elements with incompatible modes. *Computers & Structures*, 140:14–22, 2014.

[46] Cameron Talischi and Glaucio H. Paulino. Addressing integration error for polygonal finite elements through polynomial projections: A patch test connection. *Mathematical Models and Methods in Applied Sciences*, 24:1701–1727, 2014.

[47] Cameron Talischi, Anderson Pereira, Ivan F. M. Menezes, and Glaucio H. Paulino. Gradient correction for polygonal and polyhedral finite elements. *International Journal for Numerical Methods in Engineering*, 102:728–747, 2015.

[48] Eugene L. Wachspress. *A Rational Finite Element Basis*. Academic Press, 1975.

[49] J. Wang and X. Ye. A weak galerkin finite element method for second-order elliptic problems. *Journal of Computational and Applied Mathematics*, 241:103–115, 2013.

[50] X. Wang, N.S. Malluwawadu, F. Gao, and T.C. McMillan. A modified weak galerkin finite element method. *Journal of Computational and Applied Mathematics*, 271:319–329, 2014.

[51] Robert Winkler. Comments on membrane locking. *Proceedings in Applied Mathematics and Mechanics*, 10:229–230, 2010.

Brian Doran Giffin
December 2017
Civil and Environmental Engineering

A Polytopal Element Framework for
Improved Solution Accuracy and Robustness

Abstract

The abstract that is submitted to UMI must be formatted as shown in the example here. The body of the abstract cannot exceed 350 words. It should be in typewritten form, double-spaced, and on bond paper. It is important to write an abstract that gives a clear description of the content and major divisions of the dissertation, since UMI will publish the abstract exactly as submitted. Students completing their requirements under Plan A should provide extra copies of the typed summary for use by the dissertation committee during the examination.

The abstract that is submitted to UMI must be formatted as shown in the example here. The body of the abstract cannot exceed 350 words. It should be in typewritten form, double-spaced, and on bond paper. It is important to write an abstract that gives a clear description of the content and major divisions of the dissertation, since UMI will publish the abstract exactly as submitted. Students completing their requirements under Plan A should provide extra copies of the typed summary for use by the dissertation committee during the examination.

The abstract that is submitted to UMI must be formatted as shown in the example here. The body of the abstract cannot exceed 350 words. It should be in typewritten form, double-spaced, and on bond paper. It is important to write an abstract that gives a clear description of the content and major divisions of the dissertation, since UMI will publish the abstract exactly as submitted. Students completing their requirements under Plan A should provide extra copies of the typed summary for use by the dissertation committee during the examination.

The abstract that is submitted to UMI must be formatted as shown in the example here. The body of the abstract cannot exceed 350 words. It should be in typewritten form,

form, double-spaced, and on bond paper. It is important to write an abstract that gives a clear description of the content and major divisions of the dissertation, since UMI will publish the abstract exactly as submitted. Students completing their requirements under Plan A should provide extra copies of the typed summary for use by the dissertation committee during the examination.